

Spatial Control of Neuronal Metabolism Through Glucose-Mediated Mitochondrial Transport Regulation

Anamika Agrawal¹, Gulcin Pekkurnaz^{2*}, Elena F. Koslover^{1*}

***For correspondence:**

gpekkurnaz@ucsd.edu (GP);

ekoslover@ucsd.edu (EFK)

¹Department of Physics, University of California, San Diego, La Jolla CA 92130; ²Section of Neurobiology, Division of Biological Sciences, University of California, San Diego, La Jolla CA 92130

Abstract Eukaryotic cells modulate their metabolism by organizing metabolic components in response to varying nutrient availability and energy demands. In rat axons, mitochondria respond to glucose levels by halting active transport in high glucose regions. We employ quantitative modeling to explore physical limits on spatial organization of mitochondria and localized metabolic enhancement through regulated stopping of processive motion. We delineate the role of key parameters, including cellular glucose uptake and consumption rates, that are expected to modulate mitochondrial distribution and metabolic response in spatially varying glucose conditions. Our estimates indicate that physiological brain glucose levels fall within the limited range necessary for metabolic enhancement. Hence mitochondrial localization is shown to be a plausible regulatory mechanism for neuronal metabolic flexibility in the presence of spatially heterogeneous glucose, as may occur in long processes of projection neurons.

22 These findings provide a framework for the control of cellular bioenergetics through
23 organelle trafficking.

25 Introduction

26 Cellular metabolism comprises an intricate system of reactions whose fine-tuned control
27 is critical to cell health and function. A number of quantitative studies have focused on
28 metabolic control through modulating reactant and enzyme concentrations and turnover
29 rates [*Grima and Schnell (2006)*; *Amar et al. (2008)*]. However, these studies generally
30 neglect the spatial organization of metabolic components within the cell. By localizing
31 specific enzymes in regions of high metabolic demand [*Laughton et al. (2007)*; *Zecchin*
32 *et al. (2015)*], as well as clustering together consecutively acting enzymes [*O'Connell et al.*
33 *(2012)*], cells have the potential to substantially enhance their metabolism.

34 Spatial organization is particularly critical in highly extended cells, such as mammalian
35 neurons, whose axons can grow to lengths on the meter scale. Metabolic demand in
36 neurons is spatially and temporally heterogeneous, with especially rapid ATP turnover
37 found in the presynaptic boutons [*Rangaraju et al. (2014)*], and ATP requirements peaking
38 during synaptic activity and neuronal firing [*Shulman et al. (2004)*; *Ferreira et al. (2011)*;
39 *Weisová et al. (2009)*]. Neurons rely primarily on glucose as the energy source for meeting
40 these metabolic demands [*Peppiatt and Attwell (2004)*]. Due to the long lengths of neural
41 processes, the glucose supply can vary substantially over different regions of the cell
42 [*Ferreira et al. (2011)*; *Weisová et al. (2009)*; *Hall et al. (2012)*]. In myelinated neurons,
43 for instance, it has been speculated that glucose transport into the cell is localized
44 primarily to narrow regions around the nodes of Ranvier [*Magnani et al. (1996)*; *Harris*
45 *and Attwell (2012)*; *Rosenbluth (2009)*], which can be spaced hundreds of microns apart
46 [*Ibrahim et al. (1995)*; *Butt et al. (1998)*]. Glucose transporters in neurons have also been
47 shown to dynamically mobilize to active synapses, providing a source of intracellular

glucose heterogeneity [Ashrafi et al. (2017)]. Furthermore, varying levels of activity in the mammalian brain may lead to varying extracellular glucose levels, resulting in spatially heterogeneous nutrient access [Hawkins et al. (1979)]. Individual axons have been shown to span across multiple regions of the brain [Matsuda et al. (2009)], enabling them to encounter regions with different glucose concentrations.

Most ATP production in neurons occurs within mitochondria: motile organelles that range from interconnected networks to individual globular structures that extend throughout the cell. As energy powerhouses and metabolic signaling centers of the cell, mitochondria are critical for neuronal health [Nunnari and Suomalainen (2012)]. Their spatial organization within the neuron plays a pivotal role in growth and cell physiology [Li et al. (2004)]. Defects in mitochondrial transport are involved in the pathologies of several neurological disorders such as peripheral neuropathy and Charcot-Marie-Tooth disease [Baloh (2008); Baloh et al. (2007)].

A number of studies have shown that mitochondria are localized preferentially to regions of high metabolic demand, such as the synaptic terminals [Li et al. (2004); Chang and Reynolds (2006)]. Such localization can occur via several molecular mechanisms, mediated by the Miro-Milton mitochondrial motor adaptor complex that links mitochondria to the molecular motors responsible for transport [Mishra and Chan (2016)]. Increased Ca^{2+} levels at active synapses lead to loading of calcium binding sites on Miro, releasing mitochondria from the microtubule and thereby halting transport [Wang and Schwarz (2009); MacAskill et al. (2009)]. High glucose levels can also lead to stalling, through the glycosylation of motor adaptor protein Milton by the glucose-activated enzyme O-GlcNAc transferase (OGT) [Pekkurnaz et al. (2014)]. This mechanism has been shown to lead to mitochondrial accumulation at glucose-rich regions in cultured neurons [Pekkurnaz et al. (2014)]. It is postulated to regulate mitochondrial spatial distribution, allowing efficient metabolic response to heterogeneous glucose availability.

Mitochondrial positioning relies on an interplay between heterogeneously distributed diffusive signaling molecules (such as Ca^{2+} and glucose), their consumption through

76 metabolic and other pathways, and their effect on motor transport kinetics. While the bio-
 77 chemical mechanisms and physiological consequences of mitochondrial localization have
 78 been a topic of much interest in recent years [*MacAskill and Kittler (2010); Mishra and*
 79 *Chan (2016)*], no quantitative framework for this phenomenon has yet been developed.

80 In this work we focus on glucose-mediated regulation of mitochondrial transport,
 81 developing quantitative models to examine the consequences of this phenomenon for
 82 metabolism under spatially varying glucose conditions. Our approach relies on a reaction-
 83 diffusion formalism, which describes the behavior of species subject to both consumption
 84 and diffusion. Reaction-diffusion systems have been applied to describe the spatial or-
 85 ganization of a broad array of cellular processes [*Kondo and Miura (2010)*], ranging from
 86 protein oscillations in *E. coli* [*Howard et al. (2001)*], to coordination of mitotic signalling
 87 [*Chang and Ferrell Jr (2013)*], to pattern formation in developing embryos [*Bunow et al.*
 88 *(1980); Gregor et al. (2005)*]. The response of actively moving particles to spatially het-
 89 erogeneous, diffusive regulators has also been extensively investigated in the context
 90 of chemotaxis [*Van Haastert and Devreotes (2004)*]. In contrast to most chemotactic
 91 cells, however, mitochondria have no currently known mechanism for directly sensing
 92 glucose gradients. Instead, they are expected to accumulate in response to local glucose
 93 concentration only. Our goal is to delineate the regimes in which such a crude form of
 94 chemotaxis can lead to substantial spatial organization and enhancement of metabolism.

95
 96 Specifically, we model the modulation of mitochondrial density with glucose concen-
 97 tration in a tubular axonal region, focusing on two forms of spatial heterogeneity. In
 98 one case, we consider an axonal domain between two localized regions of glucose entry,
 99 representing the internodal region between nodes of Ranvier in myelinated neurons
 100 (Fig. 1a). The second case focuses on an unmyelinated cellular region with continuous
 101 glucose permeability, embedded in an external glucose gradient (Fig. 1b). In both cases,
 102 we show that mitochondrial accumulation and enhanced metabolic flux is expected to
 103 occur over a limited range of glucose concentrations, which overlaps with physiological

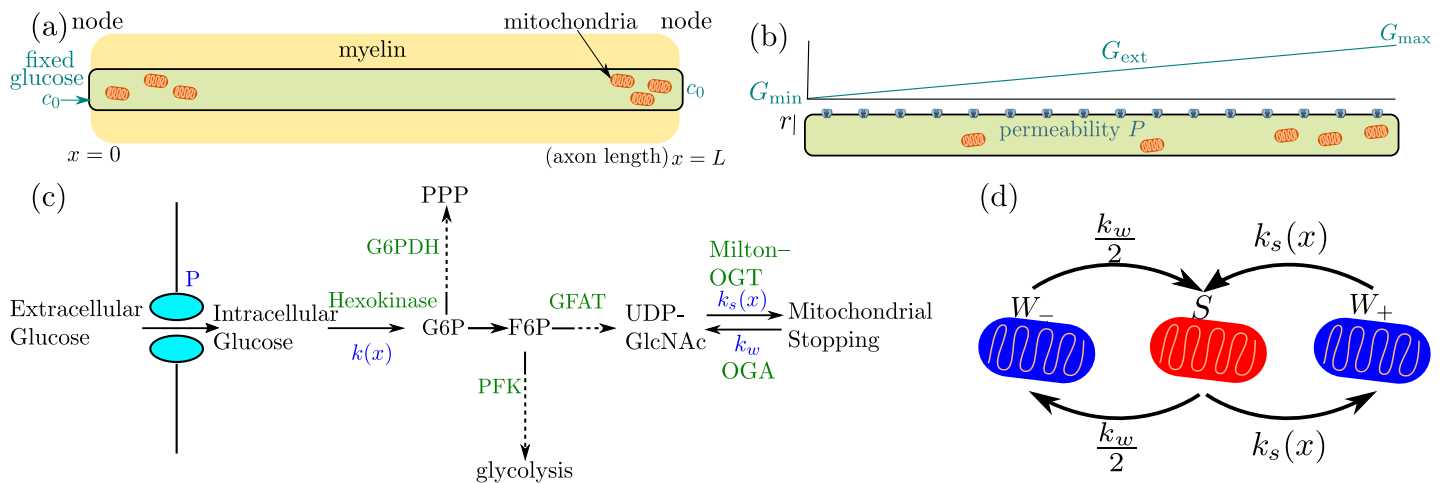


Figure 1. Schematic diagram of our simplified model for glucose-mediated mitochondrial transport regulation. (a) Myelinated axonal region, with glucose entry localized at the nodes of Ranvier. Mitochondria accumulate at nodes due to the higher glucose concentration (b) Unmyelinated axonal region, subject to a linear glucose gradient. Glucose permeability is uniform throughout, with mitochondrial accumulation occurring at the region of high external glucose (c) Key steps of the metabolic pathway linking glucose availability and mitochondrial halting. (d) Mitochondrial transport states and rates of transition between them (W_{\pm} represents retrograde and anterograde motion, S represents the stationary state).

104 brain glucose levels. Our simplified quantitative model allows identification of a handful
 105 of key parameters that govern the extent to which glucose-mediated mitochondrial halt-
 106 ing can modulate metabolism. We establish the region of parameter space where this
 107 mechanism has a substantial effect, and highlight its potential importance in neuronal
 108 metabolic flexibility and ability to respond to spatially varying glucose.

109 Results

110 Minimal model for mitochondrial and glucose dynamics

111 We begin by formulating a quantitative model to describe the spatial localization of
 112 mitochondria that halt in a glucose-dependent manner, in the presence of localized
 113 sources of glucose. This situation arises in myelinated neurons, which have glucose
 114 transporters enriched at the nodes of Ranvier, leading to highly localized sources of
 115 glucose spaced hundreds of micrometers apart within the cell [Saab et al. (2013)].

Neuronal glucose transporters are known to be bidirectional [*Simpson et al. (2007)*], allowing glucose concentration within the cell to equilibrate with external glucose. For simplicity, we assume rapid transport of glucose through these transporters, so that the internal concentration of glucose at the nodes where transporters are present is assumed to be fixed. The cellular region between two glucose sources is modeled as a one-dimensional interval of length L with glucose concentration fixed to a value c_0 at the interval boundaries (Fig. 1a). Glucose diffuses throughout this interval with diffusivity D , while being metabolized by hexokinase enzyme in the first step of mammalian glucose utilization (Fig. 1c) [*Wilson (2003)*].

The concentration of glucose is thus governed by the reaction-diffusion equation,

$$\frac{dG}{dt} = D \frac{\partial^2 G}{\partial x^2} - k(x)G(x) \quad (1)$$

where $k(x)$ describes the spatial distribution of the hexokinase enzyme as well as the rate of consumption. In the case of spatially uniform, linear consumption [$k(x) = k$, a constant] this equation can be solved directly, yielding a distribution of glucose that falls exponentially from each source boundary, with a decay length $\lambda = \sqrt{D/k}$ [*Kholodenko (2006)*].

Hexokinase 1 (HK1), the predominant form of hexokinase expressed in neurons, is known to localize preferentially to mitochondria [*John et al. (2011)*], which in mammalian axons can form individual organelles approximately $1\mu\text{m}$ in length [*Fawcett (1981)*]. We carry out numerical simulations of Eq. 1 where consumption is limited to locations of individual discrete mitochondria, represented by short intervals of length Δ . Specifically, we define the mitochondria density as $M(x) = n(x)/(\pi r^2 \Delta)$, where $n(x)$ is the number of mitochondria overlapping position x , and r is the axon radius. The phosphorylation of glucose by mitochondrial hexokinase is assumed to follow Michaelis-Menten kinetics, described by

$$k(x) = \frac{k_g M(x)}{G(x) + K_M}, \quad (2)$$

where K_M is the saturation constant and k_g is the turnover rate of glucose (per unit

time per mitochondrion). The turnover rate k_g incorporates both the catalytic rate of hexokinase and the number of hexokinase enzymes per mitochondrion. This expression reduces to the case of constant linear consumption when glucose concentration is low ($G \ll K_M$) and mitochondria are uniformly distributed throughout the region.

In general, glucose consumption depends on the location of mitochondria within the domain. Mitochondrial distribution in neurons is known to be mediated through regulation of their motor-driven motility [Chang and Reynolds (2006); Pekkurnaz et al. (2014)]. Individual mitochondria switch between processively moving and paused states, modulated by the interplay between kinesin and dynein motors and the adaptor proteins that link these motors to the mitochondria [Schwarz (2013)]. In our model, we simulate mitochondria as stochastically switching between a processive walking state that moves in either direction with velocity v and a stationary state. The rate of initiating a walk (k_w) is assumed to be constant, while the halting rate ($k_s(x)$) can be spatially heterogeneous. For simplicity, we assume the mitochondria are equally likely to move in the positive (+) or negative (-) direction each time they initiate a processive walk (Fig. 1 b).

It has recently been demonstrated that the key motor adaptor protein (Milton) is sensitive to glucose levels, halting mitochondrial motility when it is modified through O-GlcNAcylation by the OGT enzyme [Pekkurnaz et al. (2014)]. Our model employs a highly simplified description of mitochondrial dynamics, which assumes that all pauses are associated with such an O-GlcNAcylation event. Recovery from the pause at the constant rate k_w corresponds to removal of the modification through the activity of the complementary enzyme O-GlcNAcase (OGA). Although there is evidence indicating long-term glucose deprivation can reduce OGA expression [Zou et al. (2012)], for simplicity we assume in our model that OGA activity is independent of glucose levels. *In vivo* axonal mitochondria have been observed to undergo short-lived sporadic pausing while continuing to move processively in their previous anterograde or retrograde direction [Russo et al. (2009); Wang and Schwarz (2009)]. Such pauses are subsumed into an effective processive velocity v in our model. Other sources of pausing, such as Ca^{2+} -

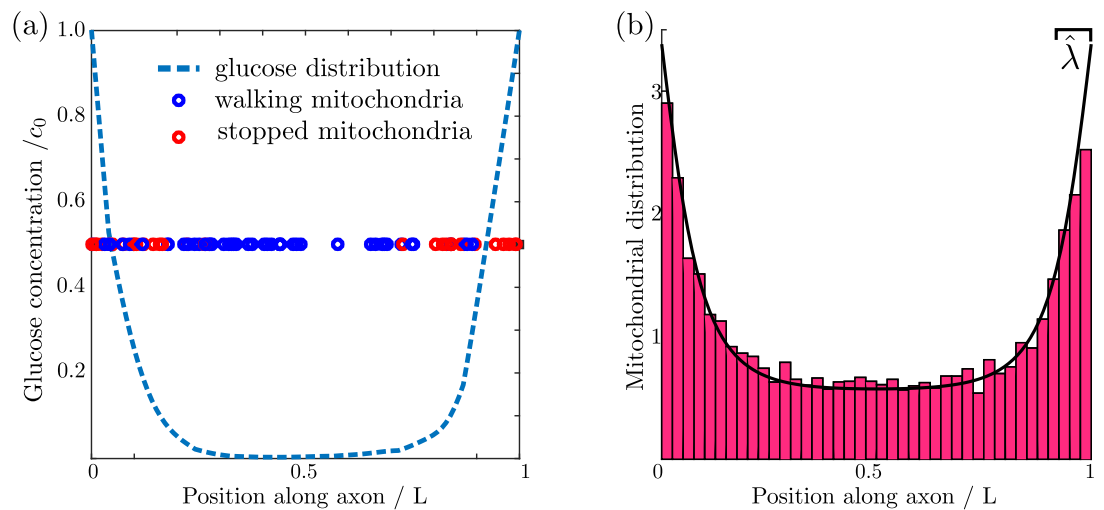


Figure 2. (a) Glucose distribution and position of individual mitochondria (b) Normalized mitochondrial distribution, $M(x)/\overline{M}$, obtained from simulating discrete mitochondrial motion (histogram compiled from 100 independent simulations), compared to numerical calculation of steady state continuous mitochondrial distribution (black curve). Results shown are for parameter values: $\hat{\lambda} = 0.08$, $\hat{c}_0 = 1$, $\hat{k}_s = 100$.

regulated motor disengagement, PINK1/Parkin-mediated detachment of motors, and anchoring to the microtubules by syntaphilin [Schwarz (2013)], are not considered here in order to focus specifically on the effect of glucose-dependent mitochondrial spatial organization.

Upon entry into the cell, the first rate-limiting step of glucose metabolism is its conversion into glucose-6-phosphate by hexokinase. Further downstream metabolic pathways split, with much of the flux going to glycolysis while a small fraction is funneled into the pentose phosphate pathway and the hexosamine biosynthetic pathway (HBP). The HBP produces UDP-GlcNAc, the sugar substrate for O-GlcNAcylation (Fig. 1c) [Hart et al. (2011)]. In our model, we assume that the rate of UDP-GlcNAc production equals the rate of glucose conversion by hexokinase, scaled by the fraction of G6P that is channeled into the hexosamine biosynthetic pathway. This assumption is valid if, at each point of pathway branching, the Michaelis-Menten saturation constants for the two branches are similar. This in fact appears to be the case for both the branching of the pentose

phosphate pathway and glycolysis from the hexosamine biosynthetic pathway which is the focus of this work (see Appendix 2). Consequently, saturation of the initial glucose conversion step will imply saturation of the entire hexosamine biosynthetic pathway. We therefore model the kinetics of Milton modification using the same Michaelis-Menten form as for hexokinase activity, with the pathway flux leading to Milton modification subsumed within a rate constant for mitochondrial stopping (k_s).

We note that the subcellular organization of the intermediates in the conversion from glucose into O-GlcNAcylated Milton is largely unknown. In our model, we make the extreme case assumption that all intermediates are localized to mitochondria, with only the initial glucose substrate capable of diffusing through the cytoplasm. We note that cytoplasmic diffusion of any of the pathway intermediates would attenuate the effect on mitochondrial localization. Our simplified model thus gives an upper limit on the extent to which mitochondria can localize at high glucose regions through the Milton modification mechanism. Following these simplified assumptions, we treat the kinetics of mitochondrial halting as dependent only on the local glucose concentration, according to the functional form

$$k_s(x) = \frac{k_s G(x)}{G(x) + K_M}, \quad (3)$$

where K_M is the Michaelis-Menten constant of hexokinase.

We proceed to evolve the simulation forward in time, with glucose consumption localized to regions within $\pm\Delta/2$ of each discrete mitochondrial position (details in Materials and Methods). A snapshot of one simulation run is shown in Fig. 2a, highlighting the accumulation of stationary mitochondria in the high glucose regions near the ends of the domain.

We are interested primarily in investigating the steady-state distribution of mitochondria and glucose in this system, averaged over all possible mitochondrial trajectories. We thus proceed to coarse-grain our model by treating the distribution of mitochondria as a continuous field $M(x) = W_+(x) + W_-(x) + S(x)$, where $W_+(x)$ is the distribution of

Table 1. Physiological parameter values estimated from published data.

cytoplasmic glucose diffusivity	D	$140\mu\text{m}^2/\text{s}$
glucose turnover per mitochondrion	k_g	$1.3 \times 10^5 \text{s}^{-1}$
axon radius	r	$0.4\mu\text{m}$
internodal distance	L	$250\mu\text{m}$
mitochondrial density	\overline{M}	$0.3\mu\text{m}^{-3}$
hexokinase Michaelis-Menten constant	K_M	0.03mM
brain glucose levels	c_0	$0.7 - 1.3\text{mM}$
ratio of stopped to moving mitochondria at high glucose	k_s/k_w	19
glucose permeability	P	$20\text{nm}/\text{s}$
glucose transporter (GLUT3) Michaelis-Menten constant	K_{MP}	3mM

Source: see Appendix 1 for details of parameter estimates.

mitochondria walking in the positive direction, $W_-(x)$ is the distribution of those walking
in the negative direction, and $S(x)$ is the distribution of stationary mitochondria. We
can then write down the coupled differential equations governing the behavior of the
mitochondrial distributions as:

$$\begin{aligned}
 \frac{dW_+}{dt} &= -v \frac{\partial W_+}{\partial x} - k_s(x)W_+ + \frac{k_w S}{2} \\
 \frac{dW_-}{dt} &= v \frac{\partial W_-}{\partial x} - k_s(x)W_- + \frac{k_w S}{2} \\
 \frac{dS}{dt} &= k_s(x)[W_+ + W_-] - k_w S.
 \end{aligned} \tag{4}$$

The glucose distribution evolves according to Eq. 1 with consumption rate $k(x)$ given by
Eq. 2. The boundary conditions at the ends of the domain are assumed to be reflective
for the mitochondrial distributions, and to have a fixed glucose concentration c_0 . The
stationary state for this system can be calculated numerically (see Materials and Meth-
ods). The formulation with a continuous mitochondrial density faithfully represents the
behavior of simulations with discrete mitochondria, as illustrated in Fig. 2b.

The steady-state spatial distribution of mitochondria and glucose in the continuous
system depend on six parameters: $k_s/k_w, K_M, c_0, D, L, k_g \overline{M}$ where \overline{M} is the average mi-

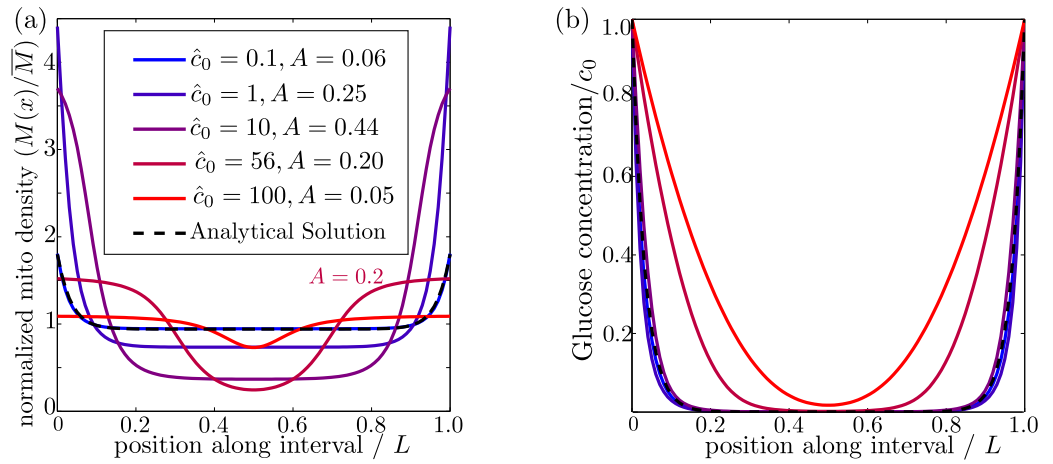


Figure 3. Effect of external glucose concentration on intracellular glucose and mitochondrial distributions. (a) Normalized mitochondrial distribution ($M(x)/\bar{M}$), for different values of edge concentration \hat{c}_0 . The curve with $\hat{c}_0 = 56$ illustrates the accumulation cutoff $A = 0.2$. (b) Glucose distribution normalized by edge concentration ($G(x)/c_0$). The black dashed line in both panels indicates the analytical solution for the low glucose limit (Materials and Methods, Eq. 13). Source data provided in "Figure 3 - source data".

221 tochondrial density in the axon (number of mitochondria per unit volume) . Estimates
 222 of physiologically relevant values are provided in Table 1. Dimensional analysis indicates
 223 that three of these parameters can be used to define units of time, length, and glucose
 224 concentration, leaving three dimensionless groups. We choose to use the following three
 225 dimensionless parameters, each of which has an intuitive physical meaning:

$$\hat{\lambda} = \sqrt{\frac{DK_M}{k_g \bar{M} L^2}}, \quad \hat{c}_0 = \frac{c_0}{K_M}, \quad \hat{k}_s = \frac{k_s}{k_w} \quad (5)$$

226 Here $\hat{\lambda}$ is the length-scale of glucose decay relative to the domain length, \hat{c}_0 is the
 227 boundary glucose concentration relative to the saturation constant K_M , and \hat{k}_s is the
 228 ratio of stopped to walking mitochondria at high glucose levels. We proceed to explore
 229 the steady-state distribution of mitochondria and glucose as a function of these three
 230 parameters.

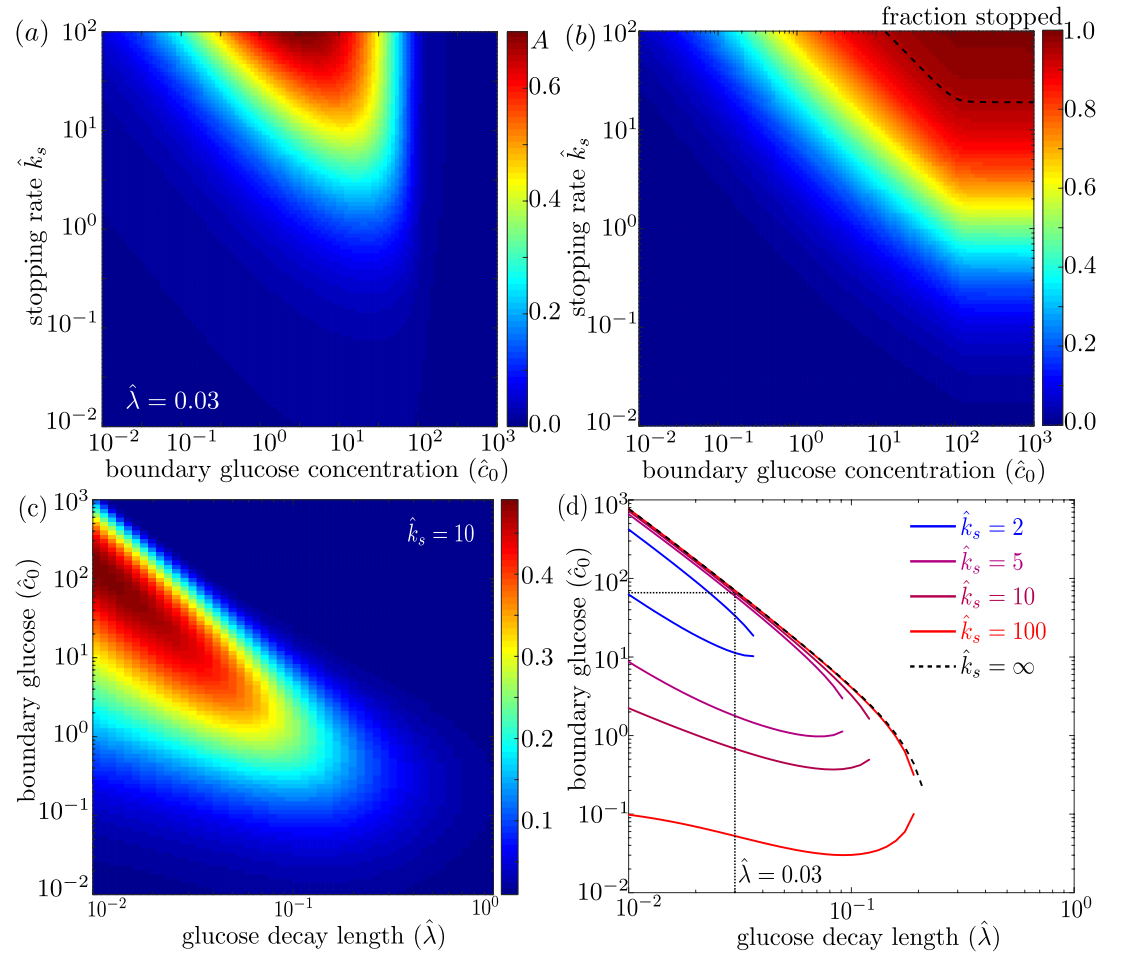


Figure 4. Effect of model parameters on mitochondrial accumulation at regions of localized glucose entry. (a) Accumulation metric as a function of boundary glucose levels and mitochondrial stopping rate. (b) Fraction of mitochondria in the stopped state. Black dashed line indicates parameters corresponding to 95% stopped mitochondria. (c) Accumulation metric as a function of glucose levels \hat{c}_0 and decay length $\hat{\lambda}$. (d) Phase diagram for mitochondrial accumulation, showing upper and lower concentration cutoffs for accumulation above the cutoff of $A_{\text{cut}} = 0.2$. Dashed black line shows limit of high stopping rate \hat{k}_s . Dotted black line indicates estimate of $\hat{\lambda}$ for physiological parameters, and corresponding upper concentration cutoff. Source data provided in "Figure 4 - source data 1-3".

Mitochondrial localization requires limited range of external glucose

In order for mitochondria to preferentially accumulate at the source of glucose via a glucose-dependent stopping mechanism, three criteria must be met. First, the glucose concentration needs to be higher at the source than in the bulk of the cell, as occurs when the decay length due to consumption is much smaller than the size of the domain ($\hat{\lambda} \ll 1$). Second, if glucose levels become too high ($\hat{c}_0 \gg 1$) then both glucose consumption rates and stopping rates of the mitochondria become saturated, leading to a flattening of glucose and mitochondrial distributions (Fig. 3). There is thus an upper limit on the possible external glucose concentrations that will yield mitochondrial localization at the edges of the domain. Finally, the mitochondria must spend a substantial amount of time in the stationary state, since walking mitochondria will be broadly distributed throughout the domain. Because the stopping rate is itself dependent on the glucose concentration, this criterion implies that very low concentrations will also not allow mitochondrial localization. Fig. 3 shows the distribution of glucose and mitochondria at different values of the external glucose \hat{c}_0 , illustrating that accumulation of mitochondria at the edges requires intermediate glucose levels.

To characterize the distribution of mitochondria along the interval, we introduce an accumulation metric A , defined by

$$A = 6\sigma^2/L^2 - 0.5$$

where σ^2 is the variance in the mitochondrial distribution. This metric scales from $A = 0$ for a uniform distribution to $A = 1$ for two narrow peaks at the domain edges. Mitochondrial distributions with several different values of the accumulation metric are shown in Fig. 3a. We use a cutoff of $A = 0.2$ to define distributions where the mitochondria are localized at the glucose source.

We explore the dependence of the mitochondrial accumulation on the three dimensionless parameters defining the behavior of the system: the stopping rate constant \hat{k}_s , the glucose decay length $\hat{\lambda}$, and the external concentration \hat{c}_0 . Because only the stopped

mitochondria localize near the glucose sources, increasing the fraction of mitochondria in the stopped state (increased \hat{k}_s) inevitably raises the overall accumulation (Fig. 4a). The fraction of mitochondria in the stopped state will depend on both \hat{k}_s and the overall levels of glucose, as dictated by \hat{c}_0 (Fig. 4b). Experimental measurements indicate that at high glucose concentrations, approximately 95% of mitochondria are in the stationary state [Pekkurnaz et al. (2014)]. We are thus interested primarily in the parameter regime of high stopping rates: $\hat{k}_s \gtrsim 10$. The limited range of concentrations that lead to mitochondrial accumulation at the edges of the domain can be seen in Fig. 4a.

For a high stopping rate ($\hat{k}_s = 10$), we then calculate the mitochondrial accumulation as a function of the remaining two parameters: $\hat{\lambda}, \hat{c}_0$. Here, again, we note that only intermediate glucose concentrations result in accumulation, with the range of concentrations becoming narrower as the decay length $\hat{\lambda}$ becomes comparable to the domain size (Fig. 4c). We can establish the concentration range within which substantial accumulation is expected, by setting a cutoff $A = 0.2$ on the accumulation metric and calculating the resulting phase diagram (Fig. 4d). Below the lower concentration cutoff, insufficient mitochondria are in the stationary state and so no localization is seen. This lower cutoff disappears in the limit of infinite \hat{k}_s . At intermediate concentrations, mitochondria are localized near the domain edges. Above the upper concentration cutoff, no localization is observed due to saturation of the Michaelis-Menten kinetics.

Using empirically derived approximations for the rate of glucose consumption by mitochondria and the diffusivity of glucose in cytoplasm (see Table 1), we estimate the decay length parameter as $\hat{\lambda} \approx 0.03$. The mitochondria are then expected to localize near the glucose source only if $\hat{c}_0 < 66$. Because the saturation concentration for hexokinase is quite low ($K_M \approx 0.03\text{mM}$) [Wilson (2003)], we would expect mitochondrial accumulation for glucose concentrations below about 2 mM. We note that physiological brain glucose levels have been measured at 0.7 – 1.3mM, depending on the brain region [McNay et al. (2001)], implying that glucose-dependent halting of mitochondrial transport would be expected to result in localization of mitochondria at nodes of Ranvier.

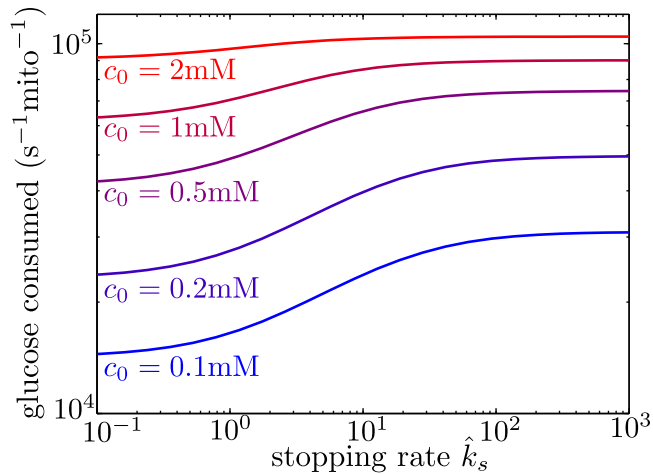


Figure 5. Mitochondrial stopping increases overall metabolic flux. Total glucose consumption per mitochondrion, averaged over the full interval, is shown for different edge glucose concentrations (c_0) as a function of the mitochondrial stopping rate \hat{k}_s . The limit of small \hat{k}_s corresponds to uniform mitochondria distribution. Parameters for the model are taken from Table I. Source data is provided in “Fig. 5 - source data”.

Glucose-dependent halting can increase metabolic flux under physiological conditions

Localizing mitochondria to the glucose entry points is expected to increase the flux of glucose entering the cell, thereby potentially enhancing the overall metabolic rate. We calculate the overall effect of transport-based regulation on the net metabolic flux within the simplified model with localized glucose entry. Fig. 5 shows the effect of increasing mitochondrial stopping rates (\hat{k}_s) on the total rate of glucose consumption in the interval between nodes of glucose influx. At low \hat{k}_s values, mitochondria are distributed uniformly throughout the interval. At high \hat{k}_s values and at sufficiently low glucose concentrations, the mitochondria cluster in the regions of glucose entry, increasing the overall consumption rate by up to 40% at physiologically relevant glucose levels ($c_0 = 1\text{mM}$). We note that in hypoglycemic conditions, glucose levels can drop to 0.1mM [Silver and Erecinska (1994)], further increasing the magnitude of this effect.

296 In the case of limited glucose transport into the cell, intracellular glucose levels could
 297 be significantly below the concentrations outside the cell. Measurements of intracellular
 298 glucose in a variety of cultured mammalian cell types indicate internal concentrations
 299 within the range of 0.07 – 1mM, up to an order of magnitude lower than glucose con-
 300 centrations in the medium [*John et al. (2008)*]. However, neuronal cells are known to
 301 express a particularly efficient glucose transporter (GLUT3) [*Simpson et al. (2008)*], and
 302 these transporters have been shown to be highly concentrated near the nodes of Ranvier
 303 [*Magnani et al. (1996); Rosenbluth (2009)*]. We therefore assume that glucose import
 304 into the nodes is not rate limiting for myelinated neurons in physiological conditions.
 305 Introducing a finite rate of glucose transport would effectively decrease the intracellular
 306 glucose concentration at the nodes c_0 , increasing the enhancement in metabolic flux
 307 due to mitochondrial localization. In subsequent sections, we explore the role of limited
 308 glucose import in unmyelinated axons with spatially uniform glucose permeability.

309 **Model for spatial organization in a glucose gradient**

310 Extracellular brain glucose levels exhibit substantial regional variation, particularly under
 311 hypoglycemic conditions where more than ten-fold differences in local glucose concen-
 312 trations have been reported [*Paschen et al. (1986)*]. Because individual neurons can
 313 traverse multiple different brain regions [*Matsuda et al. (2009)*], a single axon can be
 314 subjected to heterogeneous glucose levels along its length. This raises the possibility
 315 that glucose-dependent mitochondrial localization can play a role in neuronal metabolic
 316 flexibility even in the case where glucose entry into the cell is not localized to distinct
 317 nodes. We thus extend our model to quantify the distribution of mitochondria in an axon
 318 with limited but spatially uniform glucose permeability that is subjected to a gradient
 319 of external glucose. This situation is relevant, for instance, to unmyelinated neurons in
 320 infant brains, as well as to *in vitro* experiments with neurons cultured in a glucose gradient
 321 [*Pekkurnaz et al. (2014)*].

322 In this model, the extracellular environment provides a continuous source of glucose

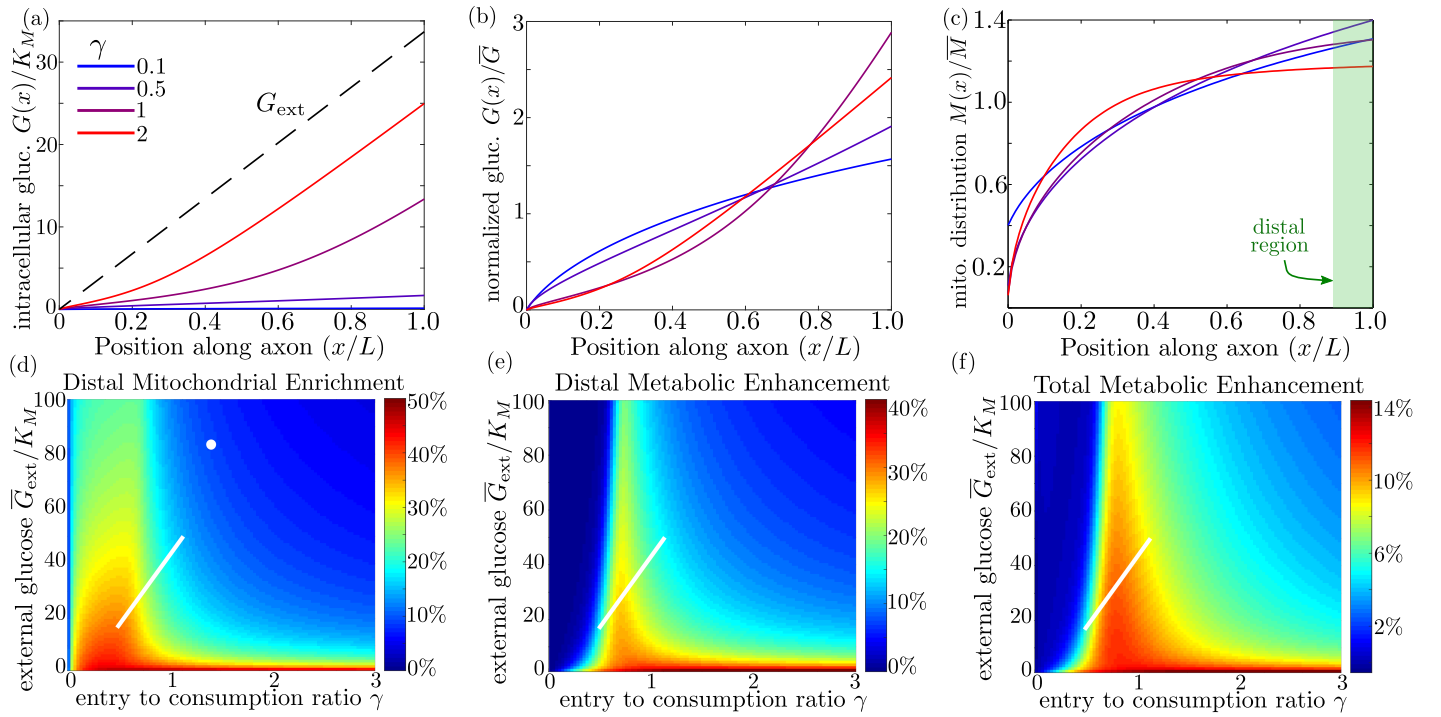


Figure 6. Mitochondrial and glucose organization in a region with uniform glucose permeability, subjected to a gradient of external glucose. (a) Internal glucose levels for the steady state solution with $\bar{G}_{\text{ext}}/K_M = 17$ ($\bar{G}_{\text{ext}} = 0.5$ mM) and varying ratios of entry to consumption rate γ . Black dashed line shows external glucose levels. (b) Corresponding normalized distribution of internal glucose. (c) Corresponding normalized mitochondrial distribution. Shaded box indicates distal region used for calculating mitochondrial enrichment and metabolic enhancement in panels d-e. (d) Mitochondrial enrichment in the distal 10% of the interval at highest external glucose, compared to a uniform distribution. White dot marks estimated parameter values for neuronal cell culture experiments ($\bar{G}_{\text{ext}} = 2.5$ mM). (e) Enhancement in metabolic flux in the distal region at high glucose, compared to a uniform mitochondrial distribution. (f) Enhancement in metabolic flux over full interval. White line in (d-f) shows estimated parameter range for physiological glycemic levels $0.5\text{mM} < \bar{G}_{\text{ext}} < 1.5\text{mM}$. Parameter values $\hat{k}_s = 19$, $\Delta\hat{G}_{\text{ext}} = 2$ used throughout. Source data is provided in “Fig. 6 - source data 1-3”.

Figure 6-Figure supplement 1. High stopping rate limit for model with uniform glucose permeability. For the high k_s limit, we show (a) mitochondrial enrichment in the distal region and (b) metabolic enhancement in the distal region. In this limit, mitochondrial accumulation occurs for arbitrarily low values of γ as nearly all mitochondria are in the stopped state even at very low internal glucose concentrations. However, metabolic enhancement still occurs only within a narrow range of γ values.

whose influx is limited by the permeability of the cell membrane. Intracellular glucose dynamics are then defined by the reaction-diffusion equation

$$\frac{dG}{dt} = D \frac{\partial^2 G}{\partial x^2} - k(x)G + P(x) (G_{\text{ext}}(x) - G), \quad (6)$$

where the first term corresponds to diffusive glucose spread, the second to a spatially varying metabolism of glucose, and the third to the entry of glucose into the cell. Here, G_{ext} is the external glucose concentration, and $P(x)$ is the membrane permeability to glucose, which we assume to depend in a Michaelis-Menten fashion on the difference between external and internal glucose concentration:

$$P(x) = \frac{(2/r)PK_{MP}}{K_{MP} + |G_{\text{ext}}(x) - G(x)|}, \quad (7)$$

where P is the spatially uniform permeability constant in units of length per time. This functional form incorporates two known features of glucose transporters: (1) they are bidirectional, so that the overall flux through the transporter at low glucose levels should scale linearly with the difference between external and internal glucose [Carruthers (1990)]; (2) neuronal glucose transporters saturate at high glucose levels (GLUT3 $K_{MP} \approx 3\text{mM}$ [Maher et al. (1996)], with an even higher saturation constant for GLUT4 [Nishimura et al. (1993)]). When the difference in glucose levels is low, the overall flux of glucose entering the cell reduces to $P(G_{\text{ext}}(x) - G(x))$. Mitochondria dynamics are defined as before (Eq. 4), and we again assume Michaelis-Menten kinetics for glucose metabolism by hexokinase localized to mitochondria (Eq. 2).

We note that the dynamics in Eq. 6 are governed by three time-scales: the rate of glucose transport down the length of the axon, rate of glucose consumption, and rate of glucose entry. The first of these rates becomes negligibly small in the limit $L \gg \sqrt{D(G + K_M)/(k_g \overline{M})}$. Because internal glucose levels can never exceed the external concentrations, in the range where $G_{\text{ext}} < 10\text{mM}$, the rate of diffusive transport should become negligible for $L \gg 150\mu\text{m}$. In the limit where intracellular glucose is much less than K_m , this criterion reduces to $\hat{\lambda} \ll 1$, indicating that glucose diffuses over a very

small fraction of the interval before being consumed. The interval length L in this model represents an axonal length which can range over many orders of magnitude. We focus on axon lengths above several hundred microns, allowing us to neglect the diffusive transport of intracellular glucose (see Appendix 3).

The steady-state glucose profile can then be determined entirely by the local concentration of mitochondria and external glucose. For a given mitochondrial density $M(x)$ and external glucose profile $G_{\text{ext}}(x)$, the corresponding intracellular glucose concentration can be found directly by solving the quadratic steady-state version of Eq.6 without the diffusive term. However, the steady-state mitochondrial distribution cannot be solved locally, because the limited number of mitochondria within the axon couples the mitochondrial density at different positions. We thus employ an iterative approach to numerically compute the steady-state solution for both glucose and mitochondrial density under a linear external glucose gradient $G_{\text{ext}} = G_{\text{min}} + (G_{\text{max}} - G_{\text{min}})\frac{x}{L}$ (see Materials and Methods).

For parameter combinations where intracellular glucose concentrations are above K_M but well below G_{ext} , the entry and consumption processes for glucose are both saturated. There is then a steep transition between two different regimes. In one regime, glucose entry exceeds consumption and internal glucose levels approach the external concentrations. In the other, consumption dominates and glucose levels drop below saturating concentrations. The key dimensionless parameter governing this transition can be defined as the ratio of entry to consumption rates:

$$\gamma = \frac{2PK_M\bar{G}_{\text{ext}}}{k_g\bar{M}r(K_M + \bar{G}_{\text{ext}})}. \quad (8)$$

This ratio can be modulated in the cell either by recruiting varying amounts of glucose transporters (adjusting P) or changing the total amount of active hexokinase (adjusting $k_g\bar{M}$).

The remaining dimensionless parameters determining the behavior of this simplified model are the external glucose concentration relative to the hexokinase saturation constant ($\hat{G}_{\text{ext}} = \bar{G}_{\text{ext}}/K_M$), the relative magnitude of the glucose gradient, $\Delta\hat{G}_{\text{ext}} =$

373 $(G_{\max} - G_{\min})/\bar{G}_{\text{ext}}$, the ratio of stopped to walking mitochondria $\hat{k}_s = k_s/k_w$, and the
 374 saturation constant for glucose transporters $K_{MP}/K_M \approx 96$. The last parameter is ex-
 375 pected to remain approximately constant in neuronal cells. The average external glucose
 376 concentration and glucose gradient are expected to vary substantially depending on
 377 the glycemic environment to which the neuron is exposed. We note that $\Delta\hat{G}_{\text{ext}}$ has a
 378 maximum possible value since the minimal glucose concentration cannot drop below 0.
 379 We proceed to analyze the limiting case where the glucose gradient is as steep as possible
 380 for any given value of average external glucose ($\Delta\hat{G}_{\text{ext}} = 2$).

381 **Mitochondrial arrest enables metabolic enhancement under glucose** 382 **gradient**

383 We quantify the amount of mitochondrial accumulation at the high glucose side of
 384 the domain by calculating the total mitochondrial density within the distal 10% of the
 385 interval compared to a uniform distribution, in analogy to experimental measurements
 386 [Pekkurnaz *et al.* (2014)]. Substantial enrichment in the high glucose region occurs when
 387 glucose entry into the cell cannot keep up with consumption ($\gamma \ll 1$) and the intracellular
 388 glucose levels drop below the hexokinase saturation concentration K_M , as can be seen in
 389 the glucose and mitochondrial distributions plotted in Fig. 6a-c. The interplay between
 390 external glucose levels and the entry / consumption rates is illustrated in Fig. 6d. For
 391 external glucose concentrations well above K_M there is a sharp transition to mitochondrial
 392 enrichment at $\gamma < 1$. At the lowest levels of intracellular glucose, accumulation is again
 393 reduced because a very small fraction of mitochondria are found in the stopped state.
 394 In the limit of high k_s , mitochondrial accumulation would occur for arbitrarily low values
 395 of γ (Fig. 6S1). We note that because glucose entry and turnover are much faster than
 396 diffusive spread for biologically relevant parameter regimes, the model results do not
 397 depend on the cell length L (Appendix 3).

398 Experimental measurements of mitochondrial enrichment in cultured neurons sub-
 399 jected to a gradient of 0 to 5mM glucose have indicated an approximately 20% enrichment

in mitochondrial counts at the axonal region exposed to high glucose. We note that using published estimates of typical glucose permeability and mitochondrial glucose turnover for mammalian cells (Table 1) yields a ratio of entrance and consumption rates of $\gamma \approx 1.9$ for this experimental system. Because this ratio is above 1, we would not expect to see substantial mitochondrial enrichment. To result in the experimentally observed enrichment at high glucose, the ratio γ would need to be reduced by approximately a factor of 2, implying the existence of additional regulatory mechanisms. Modulation of γ could be achieved by either decreasing the number of glucose transporters in the cell (reducing P) or upregulating total hexokinase levels (increasing k_g). Neurons are believed to regulate both the density of glucose transporters and hexokinase activity in response to external glucose concentrations and varying metabolic demand [Fujii and Beutler (1985); Robey et al. (1999); Duelli and Kuschinsky (2001)]. In particular, adaptation to glycemic levels well above physiological values, as well as possibly reduced synaptic activity in a cultured environment, may result in downregulation of glucose transporters, lowering the value of γ . The discrepancy between model prediction and observed mitochondrial accumulation highlights the existence of additional regulatory pathways not included in the current model whose role could be explored in further studies that directly quantify glucose entry and consumption rates in cultured neurons.

Physiological brain glucose levels have been measured at 0.7mM - 1.3mM [McNay et al. (2001)], with hypoglycemic levels dipping as low as 0.1mM and hyperglycemic levels rising up to 4mM [Silver and Erecinska (1994)]. Axons that stretch across different brain regions with varying glucose levels can thus be subject to a glucose gradient with \bar{G}_{ext} on the order of 1mM (white line on Fig. 6d). We note that the physiological range overlaps substantially with the region of high mitochondrial accumulation, indicating that glucose-dependent halting can modulate mitochondrial distribution under physiologically relevant glycemic levels.

By accumulating mitochondria at the cellular region subjected to higher external glucose, the metabolic flux in that region can be substantially enhanced. In Fig. 6e we plot

the enhancement in glucose consumption rates (compared to the case with uniformly distributed mitochondria) within the 10% of cellular length subjected to the highest glucose concentrations. Metabolic enhancement occurs within a narrow band of the γ parameter. The drop-off in enhancement at low values of the internal glucose concentration (low γ) is due to the coupling between glucose levels and mitochondrial localization. Specifically, mitochondrial accumulation at the region subject to high glucose concentration increases the local rate of consumption in that region, driving down local internal glucose levels. Consequently, the difference in internal glucose concentrations between the two ends of the cell is decreased when internal levels fall substantially below K_M (Fig. 6b), reducing the enhancement of metabolic flux. Although mitochondrial accumulation decreases metabolic flux in the low glucose region, the total rate of glucose consumption integrated throughout the cell is enhanced by up to approximately 14% when $\gamma \approx 1$ (Fig. 6f).

It is interesting to note that the typical physiological range of external glucose levels spans the narrow band of parameter space where metabolic enhancement is expected (white lines on Fig. 6e,f). These results implicate glucose-dependent mitochondrial stopping as a quantitatively plausible mechanism of metabolic flexibility, increasing metabolism in regions with high nutrient availability for axonal projections that span between hypoglycemic and euglycemic regions. The magnitude of this effect can be tightly controlled by the cell through modulating overall rates of glucose entry and consumption. Thus, by coupling mitochondrial transport to local glucose levels, whole-cell changes in hexokinase or glucose transporter recruitment can be harnessed to tune the cell's response to spatially heterogeneous glucose concentrations.

Discussion

The minimal model described here provides a quantitative framework to explore the interdependence of glucose levels and mitochondrial motility and their combined effect on neuronal metabolic flux. Glucose-mediated halting of mitochondrial transport is shown to be a plausible regulatory mechanism for enhancing metabolism in cases with

455 spatially heterogeneous glucose availability in the neuron.

456 We have quantitatively delineated the regions in parameter space where such a
 457 mechanism can have a substantial effect on mitochondrial localization and metabolic
 458 flux. Specifically, mitochondrial positioning requires both sufficient spatial variation
 459 in intracellular glucose and sufficiently low absolute glucose levels compared to the
 460 saturation constant of the hexokinase enzyme. In the case of tightly localized glucose
 461 entry (as at the nodes of Ranvier), intracellular spatial heterogeneity requires a small
 462 value of the dimensionless length scale for glucose decay ($\hat{\lambda} = \sqrt{DK_M/k_g \bar{M} L^2} \ll 1$). For
 463 physiologically estimated values, mitochondrial localization to the nodes is expected to
 464 occur for glucose levels below approximately 2mM, comparable to physiological brain
 465 glucose concentrations [McNay et al. (2001); John et al. (2008)]. In the case where glucose
 466 can enter homogeneously throughout the cell surface (as with unmyelinated axons),
 467 heterogeneity can arise from an external glucose gradient. We show that metabolic
 468 enhancement through mitochondrial positioning occurs in a narrow range of the key
 469 parameter $\gamma = (2PK_{MP}\bar{G}_{\text{ext}})/(k_g\bar{M}(K_{MP} + \bar{G}_{\text{ext}}))$, which describes the ratio of glucose
 470 entry to glucose metabolism, and that this narrow range intersects with physiological
 471 estimates.

472 The model developed here is intentionally highly simplified, encompassing a minimal
 473 set of parameters necessary to describe glucose-dependent mitochondrial localization.
 474 Other regulatory pathways that determine mitochondrial positioning are not included
 475 in this basal model. In particular, we do not consider here calcium-based transport
 476 regulation, which is known to localize mitochondria to regions of synaptic activity [Zhang
 477 et al. (2010); Wang and Schwarz (2009); MacAskill and Kittler (2010); MacAskill et al.
 478 (2009)]. Upregulating OGT signaling in cultured cells has been shown to decrease the
 479 fraction of motile mitochondria by a factor of three, while reducing endogenous OGT
 480 nearly doubles the motile fraction, indicating that a substantial number of stationary
 481 mitochondria are stopped as a result of OGT activity [Pekkurnaz et al. (2014)]. Our model
 482 assumes the extreme case where all stopping events are triggered in a glucose-dependent

483 manner, thereby isolating the effect of glucose heterogeneity. Stopping mechanisms
 484 dependent on neuronal firing activity could alter mitochondrial distribution in concert
 485 with glucose-dependent halting, increasing the density of mitochondria at presynaptic
 486 boutons or near areas of localized calcium influx as at the nodes of Ranvier [Zhang *et al.*
 487 (2010)]. We note that mitochondria have previously been shown to accumulate at spinal
 488 nodes of Ranvier in response to neuronal firing activity [Fabricius *et al.* (1993); Zhang
 489 *et al.* (2010)]. The mechanism described here provides an additional driving force for
 490 mitochondrial localization near the nodes even in quiescent neurons.

491 Additional metabolic feedback loops, not included in our model, may result in a more
 492 complex dependence of mitochondrial stopping on glucose concentration. In particu-
 493 lar, both the pentose phosphate pathway and glycolysis generate intermediates that
 494 feed back into UDP-GlcNAc production by the hexosamine biosynthetic pathway [Kruger
 495 *and von Schaewen* (2003); Shirato *et al.* (2010)]. Furthermore, several of the enzymes
 496 involved in the metabolic pathways linking glucose levels to Milton O-GlcNacylation may
 497 be regulated in a glucose-dependent manner. For example, the activity of the fructose-6-
 498 phosphate metabolizing enzyme GFAT is believed to be regulated by intermediates in the
 499 hexosamine pathway [Traxinger *and Marshall* (1991)] and O-GlcNAc transferase (OGT)
 500 itself is directly regulated by UDP-GlcNAc levels [Hart *et al.* (2007)]. Other enzymes, such
 501 as the de-GlcNAcyating enzyme OGA exhibit long term regulation of expression in re-
 502 sponse to altered glucose levels [Zou *et al.* (2012)]. These regulatory mechanisms provide
 503 additional potential routes of metabolic control through mitochondrial positioning.

504 Several key parameters that regulate mitochondrial localization in response to glu-
 505 cose heterogeneity can be dynamically regulated in neurons. Specifically, the rate of
 506 glucose consumption ($k_g \overline{M}$) can be tuned by modulating the concentration or activity of
 507 hexokinase within mitochondria or by altering total mitochondrial size and number. This
 508 parameter controls both the glucose decay length $\hat{\lambda}$ in the case of localized glucose influx
 509 and the ratio of glucose entry to consumption γ in the case of spatially distributed entry.
 510 We note that our model assumes hexokinase to be localized exclusively to mitochondria.

511 The predominant form of hexokinase in the brain (HK1) is known to bind reversibly to the
 512 mitochondrial membrane, with exchange between a mitochondria-bound and a cytoplas-
 513 mic state believed to contribute to the regulation of its activity [*Golestani et al. (2007)*].
 514 Release of hexokinase into the cytoplasm would result in more spatially uniform glucose
 515 consumption, negating the metabolic enhancement achieved through mitochondrial
 516 localization.

517 An additional parameter known to be under regulatory control is the rate of glucose
 518 entry into the neuron (P). The glucose transporters GLUT3 [*Simpson et al. (2008)*; *Duelli*
 519 *and Kuschinsky (2001)*; *Weisová et al. (2009)*] and GLUT4 [*Ashrafi et al. (2017)*] have been
 520 shown to be recruited to the plasma membrane in response to neuronal firing activity.
 521 Interestingly, transporter densities are themselves spatially heterogeneous, concentrating
 522 near regions of synaptic activity [*Ashrafi et al. (2017)*; *Ashrafi and Ryan (2017)*]. The
 523 model described in this work quantifies the extent to which a locally increased glucose
 524 influx can enhance total metabolic flux, given the ability of mitochondria to accumulate at
 525 regions of high intracellular glucose.

526 A number of possible feedback pathways linking glucose distribution and mitochon-
 527 drial positioning are not included in our basic model. For instance, hexokinase release
 528 from mitochondria into the cytoplasm (potentially altering k_g) is known to be triggered at
 529 least in part by glucose-6-phosphate, the first byproduct in glucose metabolism [*Crane*
 530 *and Sols (1954)*]. Chronic hypoglycemia has been linked to an upregulation in GLUT3
 531 in rat neurons [*Uehara et al. (1997)*], which would in turn lead to an increased glucose
 532 uptake (P). The fraction of glucose funneled into the hexosamine biosynthetic pathway
 533 (incorporated within k_s) can also be modified through feedback inhibition of GFAT by the
 534 downstream metabolic product UDP-GlcNAc [*Li et al. (2007)*]. Such feedback loops imply
 535 that several of our model parameters (P , k_g , k_s) are themselves glucose-dependent and
 536 may become spatially non-uniform in response to heterogeneous glucose. Incorporating
 537 these effects into a spatially resolved model of metabolism would require quantifying
 538 the dynamics of both the feedback pathways and mitochondrial positioning, and forms a

539 promising avenue for future study.

540 Control of glucose entry and consumption underlies cellular metabolic flexibility, and
 541 defects in the associated regulatory pathways can have grave consequences for neuronal
 542 health. Misregulation of hexokinase has been highlighted as a contributor to several
 543 neurological disorders, ranging from depression [*Regenold et al. (2012)*] to schizophrenia
 544 [*Shan et al. (2014)*]. Neuronal glucose transporter deficiency has been linked to autism
 545 spectrum disorders [*Zhao et al. (2010)*] and Alzheimer's disease [*Liu et al. (2008)*]. Further-
 546 more, defects in mitochondrial transport, with the consequent depletion of mitochondria
 547 in distal axonal regions, contribute to peripheral neuropathy disorders [*Baloh (2008)*].

548 Glucose-dependent mitochondrial localization provides an additional layer of control,
 549 beyond conventionally studied regulatory mechanisms, which allows the cell to respond to
 550 spatial heterogeneity in glucose concentration. Our analysis paves the way for quantitative
 551 understanding of how flexible regulation of metabolism can be achieved by controlling
 552 the spatial distribution of glucose entry and consumption.

553 **Materials and Methods**

554 Source code (in MATLAB [*MATLAB (2015)*]) for all simulations and numerical calculations
 555 is available at: <https://github.com/lenafabr/mitoManuscriptCodes>.

556 **Discrete mitochondria simulations**

557 We simulate the internodal space of the axon, between localized nodes of glucose entry, as
 558 a one-dimensional domain for a reaction diffusion system with motile reaction sinks. The
 559 glucose concentration field is discretized over 100 equidistant points along the domain.
 560 Its dynamics are governed by the reaction diffusion equation (Eq. 1), evolved forward over
 561 time-steps of δt using the forward Euler method. Because forward Euler methods have
 562 stringent conditions for stability and convergence, we use a time-step that is much smaller
 563 than both the glucose decay time-scale and the time-scale associated with diffusion over
 564 our spatially discretized grid (see below).

565 The number of mitochondria in the domain is calculated according to $N = \overline{M} L \pi r^2 \approx 38$,
 566 where the mitochondrial density \overline{M} , internodal distance L , and axonal radius r are
 567 estimated from published data (Table 1; Appendix 1). The mitochondria are treated as
 568 discrete intervals of length $\Delta = 1\mu\text{m}$, with the position of each mitochondrial center
 569 updated at each timestep. Over each time step, every motile mitochondrion moves
 570 a distance of $\pm v \delta t$, (with transport velocity $v = 1\mu\text{m/s}$) and switches to a stationary
 571 state with probability $1 - \exp(-k_s \delta t)$, where $k_s(x)$ is a function of the center position
 572 of that mitochondrion (Eq. 3). Mitochondria that reach within a distance of $\Delta/2$ from
 573 the ends of the domain are reflected, reversing their velocity while remaining motile.
 574 Analogously, every stationary mitochondrion switches to a motile state on each time-step
 575 with probability $1 - \exp(-k_w \delta t)$. Processive walks are initiated with equal probability in
 576 either direction.

577 At any given time, the spatial density of mitochondria is calculated from the location
 578 of mitochondrial centers at positions x_1, \dots, x_N , according to $M(x) = n(x)/(\pi r^2 \Delta)$, where

$$n(x) = \sum_{i=1}^N [\theta(x - x_i + \Delta/2) - \theta(x - x_i - \Delta/2)],$$

579 is the number of mitochondria overlapping spatial position x and θ is the Heaviside step
 580 function.

581 We integrate the simulation forward in time-steps of $\delta t = 0.2 \frac{\Delta x^2}{D}$, where Δx is the spatial
 582 discretization. This time-scale is much smaller than the relevant decay time for glucose
 583 consumption $\left[\tau_g = \left(\frac{k_g \overline{M}}{K_M} \right)^{-1} \right]$. Using these small time-steps allows for stability and
 584 robust convergence with the forward Euler method. The simulation proceeds for 10^7 steps.
 585 Simulations are repeated 100 times to obtain the histogram shown in Fig. 2. Convergence
 586 to steady-state is established by comparing to calculations with the continuum model
 587 described in the subsequent sections.

588 Mitochondrial distribution for spatially varying stopping rate

589 For an arbitrary spatial distribution of stopping rates $k_s(x)$ the corresponding steady-
 590 state mitochondrial distribution can be calculated directly by solving the equations for

mitochondrial transport (Eq. 4):

$$\begin{aligned}
 S &= \frac{k_s(x)(W_- + W_+)}{k_w} \\
 v \frac{dW_+}{dx} &= \frac{1}{2} k_s(x)(W_- - W_+) \\
 v \frac{dW_-}{dx} &= \frac{1}{2} k_s(x)(W_- - W_+).
 \end{aligned} \tag{9}$$

Because our model assumes symmetry between anterograde and retrograde mitochondrial transport, as well as equal glucose concentrations at either boundary of the domain, we take $W_- = W_+$, implying that the population of walking mitochondria must be spatially constant. Consequently, the population of stopped mitochondria is proportional to the stopping rate ($S = Ck_s(x)/k_w$). The constant C can be calculated from the normalization condition,

$$\int_0^L M(x) dx = \int_0^L [W_-(x) + W_+(x) + S(x)] dx = \overline{M}L. \tag{10}$$

The overall steady-state distribution of mitochondria is then given by,

$$M(x) = W_-(x) + W_+(x) + S(x) = \frac{\overline{M}}{1 + \frac{1}{L} \int_0^L \frac{k_s(x)}{k_w} dx} \left[\frac{k_s(x)}{k_w} + 1 \right] \tag{11}$$

.

Because the stopping rate is an explicit function of glucose concentrations $\left[k_s(x) = \frac{k_s G(x)}{K_M + G(x)} \right]$, this approach allows us to find the steady-state mitochondrial distribution for any fixed distribution of glucose.

Numerical solution for steady-state distributions with localized glucose entry

We solve for steady-state glucose and mitochondrial distributions using a numerical method that evolves the glucose concentration forward in time while explicitly setting the mitochondrial concentration to its steady-state value at each step.

The glucose distribution is initialized according to the steady-state solution for uniform consumption (Eq. 13). Mitochondrial density $M(x)$ is calculated from the glucose distribution according to Eq. 11 and Eq. 3. The glucose distribution $G(x)$, in turn, evolves

611 according to the mitochondrial distribution as given by Eq. 1 and Eq. 2 . The glucose profile
 612 is integrated forward with a timestep $\delta t = 10^{-5} L^2 / D$. The distributions are assumed to be
 613 converged once the root mean squared rate of glucose change drops below the minimal
 614 cutoff: $10^{-6} k_g \overline{M}$. Results of the continuous mitochondrial distribution model are shown
 615 to match the discrete mitochondria simulations (Fig. 2b). All subsequent analysis is done
 616 in the continuum limit.

617 **Analytical solution for low glucose limit**

618 We validate our numerical calculations by comparing to the analytically tractable solution
 619 in the limit of low glucose and nearly uniform mitochondrial distribution. In the limit of
 620 spatially uniform, linear consumption, the steady-state reaction-diffusion equation for
 621 glucose can be expressed as

$$0 = D \frac{\partial^2 G}{\partial x^2} - k G(x), \quad (12)$$

622 where $k = k_g \overline{M} / K_M$ is the constant consumption rate.

623 Assuming fixed glucose concentrations (c_0) at the boundaries of the domain, the
 624 steady-state glucose distribution is then given by

$$G(x) = \frac{c_0 \cosh(\frac{x}{\lambda})}{\cosh(\frac{L}{2\lambda})}, \quad (13)$$

625 with $\lambda = \sqrt{\frac{D}{k}}$ defining the glucose decay length-scale. This quantity is a measure of how far
 626 glucose diffusively penetrates into the domain before being consumed by hexokinase. It is
 627 scaled by the size of the domain to give the dimensionless decay length scale $\hat{\lambda} = \sqrt{\frac{DK_M}{k_g \overline{M} L^2}}$
 628 used as a key parameter in our model with localized glucose entry:

629 **Steady-state distribution with uniform permeability in the slow dif-** 630 **fusion limit**

631 For the model with spatially uniform glucose permeability, we solve directly for the steady
 632 state distributions of glucose and mitochondria in the limit of slow diffusivity. When
 633 diffusion along the domain is slow compared to the timescales of glucose consumption

634 and glucose import, the steady-state equation for glucose concentration is given by a
 635 simplified form of Eq. 6:

$$-k(x)G(x) + P(x) (G_{\text{ext}}(x) - G(x)) = 0. \quad (14)$$

636 Substituting $k(x) = \frac{k_g M(x)G(x)}{G(x)+K_M}$ and $P(x) = \frac{(2/r)PK_{MP}}{K_{MP}+|G_{\text{ext}}(x)-G(x)|}$, we get a quadratic equation in
 637 $G(x)$;

$$\left[1 - \frac{2PK_{MP}}{rk_g M}\right] G(x)^2 + \left[\frac{2PK_{MP}G_{\text{ext}}}{rk_g M} - \frac{2PK_{MP}K_M}{rk_g M} - G_{\text{ext}} - K_{MP}\right] G(x) + \left[\frac{2PK_{MP}K_M G_{\text{ext}}}{rk_g M}\right] = 0 \quad (15)$$

638 For a given mitochondrial profile, this quadratic equation is solved to find $G(x) = G(M(x))$.
 639 The mitochondrial distribution, $M(x)$ is then updated according to Eq. 11 and Eq. 3. We
 640 thus arrive at an iterative solution for $G(x)$ and $M(x)$.

641 Acknowledgments

642 We thank Saurabh Mogre for fruitful discussions, Manho Tang for numerical modeling
 643 advice, and David Kleinfeld for helpful comments on the manuscript.

References

- Amar, P., Legent, G., Thellier, M., Ripoll, C., Bernot, G., Nystrom, T., Saier, M. H., and Norris, V. (2008). A stochastic automaton shows how enzyme assemblies may contribute to metabolic efficiency. *Bmc Syst Biol*, 2(1):27.
- Ashrafi, G. and Ryan, T. A. (2017). Glucose metabolism in nerve terminals. *Curr Opin Neurobiol*, 45:156–161.
- Ashrafi, G., Wu, Z., Farrell, R. J., and Ryan, T. A. (2017). Glut4 mobilization supports energetic demands of active synapses. *Neuron*, 93(3):606–615.
- Baloh, R. H. (2008). Mitochondrial dynamics and peripheral neuropathy. *Neuroscientist*, 14(1):12–18.
- Baloh, R. H., Schmidt, R. E., Pestronk, A., and Milbrandt, J. (2007). Altered axonal mitochondrial transport in the pathogenesis of charcot-marie-tooth disease from mitofusin 2 mutations. *J Neurosci*, 27(2):422–430.
- Barazany, D., Bassar, P. J., and Assaf, Y. (2009). In vivo measurement of axon diameter distribution in the corpus callosum of rat brain. *Brain*, 132(5):1210–1220.
- Bunow, B., Kernevez, J.-P., Joly, G., and Thomas, D. (1980). Pattern formation by reaction-diffusion instabilities: Application to morphogenesis in drosophila. *J Theor Biol*, 84(4):629–649.
- Butt, A., Ibrahim, M., and Berry, M. (1998). Axon-myelin sheath relations of oligodendrocyte unit phenotypes in the adult rat anterior medullary velum. *J Neurocytol*, 27(4):205–217.
- Carruthers, A. (1990). Facilitated diffusion of glucose. *Physiol Rev*, 70(4):1135–1176.
- Chang, D. T. and Reynolds, I. J. (2006). Mitochondrial trafficking and morphology in healthy and injured neurons. *Prog Neurobiol*, 80(5):241–268.
- Chang, J. B. and Ferrell Jr, J. E. (2013). Mitotic trigger waves and the spatial coordination of the xenopus cell cycle. *Nature*, 500(7464):603.
- Crane, R. K. and Sols, A. (1954). The non-competitive inhibition of brain hexokinase by glucose-6-phosphate and related compounds. *J Biol Chem*, 210(2):597–606.

- 669 Duelli, R. and Kuschinsky, W. (2001). Brain glucose transporters: relationship to local energy demand.
670 *Physiology*, 16(2):71–76.
- 671 Duffieux, F., Van Roy, J., Michels, P. A., and Opperdoes, F. R. (2000). Molecular characterisation of the
672 first two enzymes of the pentose-phosphate pathway of trypanosoma brucei. *Journal of Biological*
673 *Chemistry*.
- 674 Fabricius, C., Berthold, C.-H., and Rydmark, M. (1993). Axoplasmic organelles at nodes of ranvier. ii.
675 occurrence and distribution in large myelinated spinal cord axons of the adult cat. *J Neurocytol*,
676 22(11):941–954.
- 677 Fawcett, D. W. (1981). *The cell: its organelles and inclusions: an atlas of fine structure*. Number 576.31
678 FAW.
- 679 Ferreira, J. M., Burnett, A. L., and Rameau, G. A. (2011). Activity-dependent regulation of surface
680 glucose transporter-3. *J Neurosci*, 31(6):1991–1999.
- 681 Fujii, S. and Beutler, E. (1985). High glucose concentrations partially release hexokinase from
682 inhibition by glucose 6-phosphate. *P Natl Acad Sci*, 82(5):1552–1554.
- 683 Golestani, A., Ramshini, H., and Nemat-Gorgani, M. (2007). A study on the two binding sites of
684 hexokinase on brain mitochondria. *Bmc Biochem*, 8(1):20.
- 685 Gregor, T., Bialek, W., van Steveninck, R. R. d. R., Tank, D. W., and Wieschaus, E. F. (2005). Diffusion
686 and scaling during early embryonic pattern formation. *P Natl Acad Sci Usa*, 102(51):18403–18407.
- 687 Grima, R. and Schnell, S. (2006). A systematic investigation of the rate laws valid in intracellular
688 environments. *Biophys Chem*, 124(1):1–10.
- 689 Hall, C. N., Klein-Flügge, M. C., Howarth, C., and Attwell, D. (2012). Oxidative phosphorylation,
690 not glycolysis, powers presynaptic and postsynaptic mechanisms underlying brain information
691 processing. *J Neurosci*, 32(26):8940–8951.
- 692 Harris, J. J. and Attwell, D. (2012). The energetics of cns white matter. *J Neurosci*, 32(1):356–371.
- 693 Hart, G. W., Housley, M. P., and Slawson, C. (2007). Cycling of o-linked β -n-acetylglucosamine on
694 nucleocytoplasmic proteins. *Nature*, 446(7139):1017.

- Hart, G. W., Slawson, C., Ramirez-Correa, G., and Lagerlof, O. (2011). Cross talk between o-glucosylation and phosphorylation: roles in signaling, transcription, and chronic disease. *Annu Rev Biochem*, 80:825–858.
- Hawkins, R., Hass, W. K., and Ransohoff, J. (1979). Measurement of regional brain glucose utilization in vivo using [2 (-14) c] glucose. *Upd Int Car*, 10(6):690–703.
- Howard, M., Rutenberg, A. D., and de Vet, S. (2001). Dynamic compartmentalization of bacteria: accurate division in e. coli. *Phys Rev Lett*, 87(27):278102.
- Ibrahim, M., Butt, A., and Berry, M. (1995). Relationship between myelin sheath diameter and internodal length in axons of the anterior medullary velum of the adult rat. *J Neurol Sci*, 133(1):119–127.
- Jacobs, J. (1988). On internodal length. *J Anat*, 157:153.
- John, S., Weiss, J. N., and Ribalet, B. (2011). Subcellular localization of hexokinases i and ii directs the metabolic fate of glucose. *PloS one*, 6(3):e17674.
- John, S. A., Ottolia, M., Weiss, J. N., and Ribalet, B. (2008). Dynamic modulation of intracellular glucose imaged in single cells using a fret-based glucose nanosensor. *Pflügers Archiv-European Journal of Physiology*, 456(2):307–322.
- Kahana, S. E., Lowry, O. H., Schulz, D. W., Passonneau, J. V., and Crawford, E. J. (1960). The kinetics of phosphoglucosomerase. *Journal of Biological Chemistry*, 235(8):2178–2184.
- Kholodenko, B. N. (2006). Cell-signalling dynamics in time and space. *Nat Rev Mol Cell Bio*, 7(3):165.
- Kondo, S. and Miura, T. (2010). Reaction-diffusion model as a framework for understanding biological pattern formation. *Science*, 329(5999):1616–1620.
- Kruger, N. J. and von Schaewen, A. (2003). The oxidative pentose phosphate pathway: structure and organisation. *Current opinion in plant biology*, 6(3):236–246.
- Laughton, J. D., Bittar, P., Charnay, Y., Pellerin, L., Kovari, E., Magistretti, P. J., and Bouras, C. (2007). Metabolic compartmentalization in the human cortex and hippocampus: evidence for a cell- and region-specific localization of lactate dehydrogenase 5 and pyruvate dehydrogenase. *Bmc Neurosci*, 8(1):35.

- Li, Y., Roux, C., Lazereg, S., LeCaer, J.-P., Laprévotte, O., Badet, B., and Badet-Denisot, M.-A. (2007). Identification of a novel serine phosphorylation site in human glutamine: fructose-6-phosphate amidotransferase isoform 1. *Biochemistry-us*, 46(45):13163–13169.
- Li, Z., Okamoto, K.-I., Hayashi, Y., and Sheng, M. (2004). The importance of dendritic mitochondria in the morphogenesis and plasticity of spines and synapses. *Cell*, 119(6):873–887.
- Liewald, D., Miller, R., Logothetis, N., Wagner, H.-J., and Schüz, A. (2014). Distribution of axon diameters in cortical white matter: an electron-microscopic study on three human brains and a macaque. *Biol Cybern*, 108(5):541–557.
- Liu, Y., Liu, F., Iqbal, K., Grundke-Iqbal, I., and Gong, C.-X. (2008). Decreased glucose transporters correlate to abnormal hyperphosphorylation of tau in alzheimer disease. *Febs Lett*, 582(2):359–364.
- MacAskill, A. F. and Kittler, J. T. (2010). Control of mitochondrial transport and localization in neurons. *Trends Cell Biol*, 20(2):102–112.
- MacAskill, A. F., Rinholm, J. E., Twelvetrees, A. E., Arancibia-Carcamo, I. L., Muir, J., Fransson, A., Aspenstrom, P., Attwell, D., and Kittler, J. T. (2009). Miro1 is a calcium sensor for glutamate receptor-dependent localization of mitochondria at synapses. *Neuron*, 61(4):541–555.
- Magnani, P., Cherian, P. V., Gould, G. W., Greene, D. A., Sima, A. A., and Brosius III, F. C. (1996). Glucose transporters in rat peripheral nerve: paranodal expression of glut1 and glut3. *Metabolism*, 45(12):1466–1473.
- Maher, F., Davies-Hill, T. M., and Simpson, I. A. (1996). Substrate specificity and kinetic parameters of glut3 in rat cerebellar granule neurons. *Biochem J*, 315(Pt 3):827.
- MATLAB (2015). *version 8.6.0 (R2015b)*. The MathWorks Inc., Natick, Massachusetts.
- Matsuda, W., Furuta, T., Nakamura, K. C., Hioki, H., Fujiyama, F., Arai, R., and Kaneko, T. (2009). Single nigrostriatal dopaminergic neurons form widely spread and highly dense axonal arborizations in the neostriatum. *J Neurosci*, 29(2):444–453.
- McNay, E. C., McCarty, R. C., and Gold, P. E. (2001). Fluctuations in brain glucose concentration during behavioral testing: dissociations between brain areas and between brain and blood. *Neurobiol Learn Mem*, 75(3):325–337.

- 750 Mironov, S. L. (2007). Adp regulates movements of mitochondria in neurons. *Biophys J*, 92(8):2944–
751 2952.
- 752 Mishra, P. and Chan, D. C. (2016). Metabolic regulation of mitochondrial dynamics. *J Cell Biol*, pages
753 jcb–201511036.
- 754 Nishimura, H., Pallardo, F., Seidner, G., Vannucci, S., Simpson, I., and Birnbaum, M. (1993). Kinetics
755 of glut1 and glut4 glucose transporters expressed in xenopus oocytes. *J Biol Chem*, 268(12):8514–
756 8520.
- 757 Nunnari, J. and Suomalainen, A. (2012). Mitochondria: in sickness and in health. *Cell*, 148(6):1145–
758 1159.
- 759 O’Connell, J. D., Zhao, A., Ellington, A. D., and Marcotte, E. M. (2012). Dynamic reorganization of
760 metabolic enzymes into intracellular bodies. *Annu Rev Cell Dev Bi*, 28:89–111.
- 761 Paschen, W., Siesjö, B., Ingvar, M., and Hossmann, K.-A. (1986). Regional differences in brain glucose
762 content in graded hypoglycemia. *Neurochem Pathol*, 5(2):131–142.
- 763 Pekkurnaz, G., Trinidad, J. C., Wang, X., Kong, D., and Schwarz, T. L. (2014). Glucose regulates
764 mitochondrial motility via mltos modification by o-glcnac transferase. *Cell*, 158(1):54–68.
- 765 Peppiatt, C. and Attwell, D. (2004). Neurobiology: feeding the brain. *Nature*, 431(7005):137.
- 766 Perge, J. A., Koch, K., Miller, R., Sterling, P., and Balasubramanian, V. (2009). How the optic nerve
767 allocates space, energy capacity, and information. *J Neurosci*, 29(24):7917–7928.
- 768 Perge, J. A., Niven, J. E., Mugnaini, E., Balasubramanian, V., and Sterling, P. (2012). Why do axons
769 differ in caliber? *J Neurosci*, 32(2):626–638.
- 770 Posakony, J. W., England, J. M., and Attardi, G. (1977). Mitochondrial growth and division during the
771 cell cycle in hela cells. *J Cell Biol*, 74(2):468–491.
- 772 Pysh, J. J. and Khan, T. (1972). Variations in mitochondrial structure and content of neurons and
773 neuroglia in rat brain: an electron microscopic study. *Brain Res*, 36(1):1–18.
- 774 Rangaraju, V., Calloway, N., and Ryan, T. A. (2014). Activity-driven local atp synthesis is required for
775 synaptic function. *Cell*, 156(4):825–835.

- 776 Regenold, W., Pratt, M., Nekkhalap, S., Shapiro, P., Kristian, T., and Fiskum, G. (2012). Mitochondrial
777 detachment of hexokinase 1 in mood and psychotic disorders: implications for brain energy
778 metabolism and neurotrophic signaling. *J Psychiatr Res*, 46(1):95–104.
- 779 Robey, R. B., Ma, J., and Santos, A. V. (1999). Regulation of mesangial cell hexokinase activity by pkc
780 and the classic mapk pathway. *Am J Physiol-renal*, 277(5):F742–F749.
- 781 Rosenbluth, J. (2009). Multiple functions of the paranodal junction of myelinated nerve fibers. *J*
782 *Neurosci Res*, 87(15):3250–3258.
- 783 Russo, G. J., Louie, K., Wellington, A., Macleod, G. T., Hu, F., Panchumarthi, S., and Zinsmaier, K. E.
784 (2009). Drosophila miro is required for both anterograde and retrograde axonal mitochondrial
785 transport. *J Neurosci*, 29(17):5443–5455.
- 786 Saab, A. S., Tzvetanova, I. D., and Nave, K.-A. (2013). The role of myelin and oligodendrocytes in
787 axonal energy metabolism. *Curr Opin Neurobiol*, 23(6):1065–1072.
- 788 Schwarz, T. L. (2013). Mitochondrial trafficking in neurons. *Cold Spring Harbor perspectives in biology*,
789 5(6):a011304.
- 790 Schwerzmann, K., Hoppeler, H., Kayar, S. R., and Weibel, E. R. (1989). Oxidative capacity of muscle
791 and mitochondria: correlation of physiological, biochemical, and morphometric characteristics. *P*
792 *Natl Acad Sci*, 86(5):1583–1587.
- 793 Shan, D., Mount, D., Moore, S., Haroutunian, V., Meador-Woodruff, J. H., and McCullumsmith, R. E.
794 (2014). Abnormal partitioning of hexokinase 1 suggests disruption of a glutamate transport
795 protein complex in schizophrenia. *Schizophr Res*, 154(1):1–13.
- 796 Sherman, D. L., Pratt, T., Garry, E. M., Ribchester, R. R., Cottrell, D. F., Fleetwood-Walker, S. M., Brophy,
797 P. J., et al. (2004). Restricted growth of schwann cells lacking cajal bands slows conduction in
798 myelinated nerves. *Nature*, 431(7005):191.
- 799 Shirato, K., Nakajima, K., Korekane, H., Takamatsu, S., Gao, C., Angata, T., Ohtsubo, K., and Taniguchi,
800 N. (2010). Hypoxic regulation of glycosylation via the n-acetylglucosamine cycle. *Journal of clinical*
801 *biochemistry and nutrition*, 48(1):20–25.
- 802 Shulman, R. G., Rothman, D. L., Behar, K. L., and Hyder, F. (2004). Energetic basis of brain activity:
803 implications for neuroimaging. *Trends Neurosci*, 27(8):489–495.

- 804 Silver, I. A. and Erecinska, M. (1994). Extracellular glucose concentration in mammalian brain:
805 continuous monitoring of changes during increased neuronal activity and upon limitation in
806 oxygen supply in normo-, hypo-, and hyperglycemic animals. *J Neurosci*, 14(8):5068–5076.
- 807 Simpson, I. A., Carruthers, A., and Vannucci, S. J. (2007). Supply and demand in cerebral energy
808 metabolism: the role of nutrient transporters. *Journal of Cerebral Blood Flow & Metabolism*,
809 27(11):1766–1791.
- 810 Simpson, I. A., Dwyer, D., Malide, D., Moley, K. H., Travis, A., and Vannucci, S. J. (2008). The facilitative
811 glucose transporter glut3: 20 years of distinction. *Am J Physiol-endoc M*, 295(2):E242–E253.
- 812 Traxinger, R. and Marshall, S. (1991). Coordinated regulation of glutamine: fructose-6-phosphate
813 amidotransferase activity by insulin, glucose, and glutamine. role of hexosamine biosynthesis in
814 enzyme regulation. *Journal of Biological Chemistry*, 266(16):10148–10154.
- 815 Uehara, Y., Nipper, V., and McCALL, A. L. (1997). Chronic insulin hypoglycemia induces glut-3 protein
816 in rat brain neurons. *Am J Physiol-endoc M*, 272(4):E716–E719.
- 817 Urbina, J. A. and Crespo, A. (1984). Regulation of energy metabolism in trypanosoma (schizotry-
818 panum) cruzi epimastigotes, i. hexokinase and phosphofructokinase. *Molecular and biochemical*
819 *parasitology*, 11:225–239.
- 820 Van Haastert, P. J. and Devreotes, P. N. (2004). Chemotaxis: signalling the way forward. *Nat Rev Mol*
821 *Cell Bio*, 5(8):626.
- 822 Vendelin, M., Kongas, O., and Saks, V. (2000). Regulation of mitochondrial respiration in heart cells
823 analyzed by reaction-diffusion model of energy transfer. *Am J Physiol-cell Ph*, 278(4):C747–C764.
- 824 Wang, X. and Schwarz, T. L. (2009). The mechanism of ca^{2+} -dependent regulation of kinesin-
825 mediated mitochondrial motility. *Cell*, 136(1):163–174.
- 826 Weisová, P., Concannon, C. G., Devocelle, M., Prehn, J. H., and Ward, M. W. (2009). Regulation of
827 glucose transporter 3 surface expression by the amp-activated protein kinase mediates tolerance
828 to glutamate excitation in neurons. *J Neurosci*, 29(9):2997–3008.
- 829 Wilson, J. E. (2003). Isozymes of mammalian hexokinase: structure, subcellular localization and
830 metabolic function. *J Exp Biol*, 206(12):2049–2057.

- 831 Xu, C.-C., Denton, K. R., Wang, Z.-B., Zhang, X., and Li, X.-J. (2016). Abnormal mitochondrial transport
832 and morphology as early pathological changes in human models of spinal muscular atrophy.
833 *Disease models & mechanisms*, 9(1):39–49.
- 834 Zecchin, A., Stapor, P. C., Goveia, J., and Carmeliet, P. (2015). Metabolic pathway compartmentaliza-
835 tion: an underappreciated opportunity? *Curr Opin Biotech*, 34:73–81.
- 836 Zhang, C. L., Ho, P. L., Kintner, D. B., Sun, D., and Chiu, S. Y. (2010). Activity-dependent regulation of
837 mitochondrial motility by calcium and na/k-atpase at nodes of ranvier of myelinated nerves. *J*
838 *Neurosci*, 30(10):3555–3566.
- 839 Zhao, Y., Fung, C., Shin, D., Shin, B.-C., Thamotharan, S., Sankar, R., Ehninger, D., Silva, A., and
840 Devaskar, S. U. (2010). Neuronal glucose transporter isoform 3 deficient mice demonstrate
841 features of autism spectrum disorders. *Mol Psychiatr*, 15(3):286.
- 842 Zou, L., Zhu-Mauldin, X., Marchase, R. B., Paterson, A. J., Liu, J., Yang, Q., and Chatham, J. C. (2012).
843 Glucose deprivation induced increase in protein o-glcnaacylation in cardiomyocytes is calcium
844 dependent. *Journal of Biological Chemistry*, pages jbc-M112.

Appendix 1

Estimating physiological parameter values

In this appendix we describe our approach to estimating the parameter values summarized in Table 1 from published experimental data.

Glucose diffusivity (D)

glucose is a small molecule of comparable molecular weight to ATP, which has a diffusion coefficient of $140\mu\text{m}^2/\text{s}$ [*Mironov (2007); Vendelin et al. (2000)*]

Glucose consumption rate per mitochondrion (k_g)

The oxidative capacity of muscle mitochondria has been measured at 5.8 mL of O_2 per min per mL mitochondria [*Harris and Attwell (2012); Schwerzmann et al. (1989)*]. We assume 6 glucose molecules are consumed per molecule of oxygen, and a volume of $0.3\mu\text{m}^3$ for globular mitochondria [*Posakony et al. (1977)*]. The corresponding glucose turnover rate of a mitochondrion is then calculated as 1.3×10^5 glucose per second per mitochondrion.

Axon radius (r)

The thickness of mammalian brain axons varies widely from $0.1\mu\text{m}$ to $10\mu\text{m}$ [*Perge et al. (2012)*]. Statistical measurements in the human brain show that most axon diameters fall below $1\mu\text{m}$, with a long-tailed distribution of substantially thicker axons [*Liewald et al. (2014)*]. We take as our estimate a median diameter of $0.8\mu\text{m}$, which is consistent with measurements in human brain regions [*Liewald et al. (2014)*], in the rat corpus collosum [*Barazany et al. (2009)*], guinea pig retinal neurons [*Perge et al. (2009)*], and in a number of other mammalian tracts [*Perge et al. (2012)*].

Internodal distance (L)

Typical internodal lengths vary widely from $200\mu\text{m}$ to $1500\mu\text{m}$ [Jacobs (1988); Sherman et al. (2004)]. We use a value of $L = 250\mu\text{m}$ as measured in the axons of rat anterior medullary velum [Ibrahim et al. (1995)].

Mitochondrial density (\overline{M})

Measurements of mitochondrial concentration in human spinal muscular nerves give a linear density of about 15 mitochondria per $100\mu\text{m}$ of axon [Xu et al. (2016)]. Similar densities are observed in Fig. 1, 2 of Ref. [Pekkurnaz et al. (2014)]. Assuming an axonal radius of $r \approx 0.4\mu\text{m}$ gives a corresponding density of $0.3\mu\text{m}^{-3}$. EM measurements in rat brain neurons indicate that mitochondria occupy approximately 8% of the neuronal cytoplasmic volume [Pysh and Khan (1972)]. Assuming a mitochondrial volume of $0.3\mu\text{m}^3$ [Posakony et al. (1977)] would give the same density estimate of 0.3 mitochondria per μm^3 .

Hexokinase Michaelis-Menten constant (K_M)

The Michaelis-Menten constant for glucose phosphorylation by the neuronal isoform of hexokinase (HKI) has been measured as $K_m = 0.03\text{mM}$ [Wilson (2003)].

Ratio of stopped to moving mitochondria (k_s/k_w)

In Ref. [Pekkurnaz et al. (2014)], mammalian neurons grown under high (30mM) glucose conditions were found to have mitochondria that spent approximately 5% of their time in motion. This fraction should correspond to $k_w/(k_s + k_w) \approx 0.05$ under our simplified model for mitochondrial motility.

Membrane permeability to glucose (P, K_{MP})

The neuronal glucose transporter GLUT3 in rat cerebellar granule neurons has been measured to have a turnover rate of $k_{\text{glut3}} = 853\text{s}^{-1}$ and a Michaelis-Menten

constant of $K_{M,\text{glut3}} = 3\text{mM}$ [Maher et al. (1996)]. In the same study, the density of GLUT3 channels was measured as 18pmol / mg cell membrane. We assume the cell membrane has a density of order 1g/cm^3 and forms a sheet of thickness 4nm. This allows us to calculate the area density of GLUT3 channels in cerebellar neurons as approximately $a = 43 \text{ transporters}/\mu\text{m}^2$.

In the case where the difference in external and internal glucose concentration (ΔG) is below $K_{M,\text{glut3}}$, we can approximate the net flux into the cell as,

$$\text{flux} = k_{\text{glut3}} a \frac{\Delta G}{K_{M,\text{glut3}}} = P \Delta G, \quad (16)$$

allowing an estimate of the permeability $P = \frac{k_{\text{glut3}} a}{K_{M,\text{glut3}}} \approx 0.02 \mu\text{m/s}$

Appendix 2

Effective Michaelis-Menten kinetics for glycosylation of Milton

We assume individual steps in glucose metabolism follow classic Michaelis-Menten kinetics, with the rate of product formation given by $dP/dt = v_i S / (K_{Mi} + S)$. We further assume that all pathways considered here are operating in steady-state, with a stationary concentration of all intermediates. When several Michaelis-Menten reactions are connected in series (eg: $A \rightarrow B \rightarrow C$), steady state requires that the dependence of final product formation C on the initial reactant A is given by,

$$\frac{dC}{dt} = \frac{v_{AB}A}{K_{AB} + A} \quad (17)$$

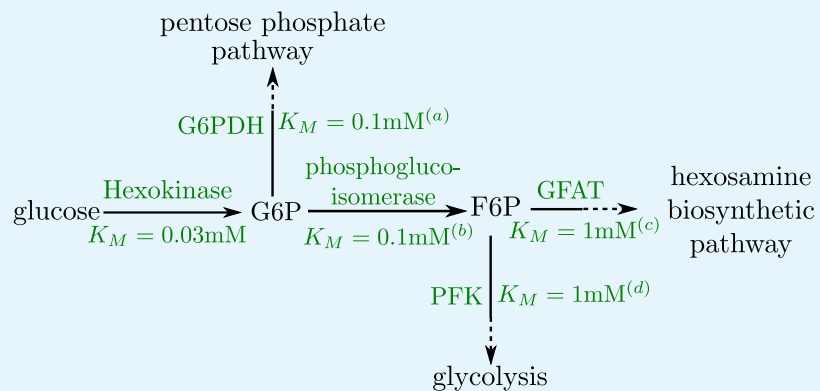
where v_{AB} , K_{AB} are the maximum rate and saturation constant for the initial $A \rightarrow B$ reaction.

If two pathways branch from a single intermediate, as occurs when the hexosamine biosynthetic pathway splits off first from the pentose phosphate pathway and then from glycolysis, then we have an additional reaction $B \rightarrow D$ that alters the rate of C formation. We make the key assumption that the saturation constants in the first step of both branching pathways are comparable ($K_{BC} \approx K_{BD}$). Steady state then requires

$$\begin{aligned} \frac{v_{AB}A}{K_{AB} + A} &= \frac{(v_{BC} + v_{BD})B}{K_{BC} + B} \\ \frac{dC}{dt} &= \left(\frac{v_{BC}}{v_{BC} + v_{BD}} \right) \frac{v_{AB}A}{K_{AB} + A} \end{aligned} \quad (18)$$

Thus, if the saturation concentrations of the splitting reactions are similar, then the formation of the final product occurs at a rate proportional to the initial substrate consumption, with the same saturation constant. As illustrated in the

pathway schematic (Appendix 2 Fig.1), the branching of both the pentose phosphate pathway and glycolysis from the pathway leading to UDP-GlcNAc formation involves similar values of the Michaelis-Menten constant. We therefore assume that the rate of Milton glycosylation by OGT (dC/dt) is proportional to the rate of initial glucose consumption by hexokinase ($|dA/dt|$). This assumption justifies our use of the same K_M for both glucose consumption and mitochondrial stopping. The fraction of metabolic flux funneled into Milton glycosylation is subsumed into the effective rate constant k_s .



Appendix 2 Figure 1. Schematic of early pathway branches in glucose metabolism, showing the branching of the pentose phosphate pathway and glycolysis from the hexosamine biosynthetic pathway that leads to UDP-GlcNAc formation. Saturation concentrations are labeled for each of the initial branching reactions. Note that in both cases, the splitting branches have comparable values of K_M .

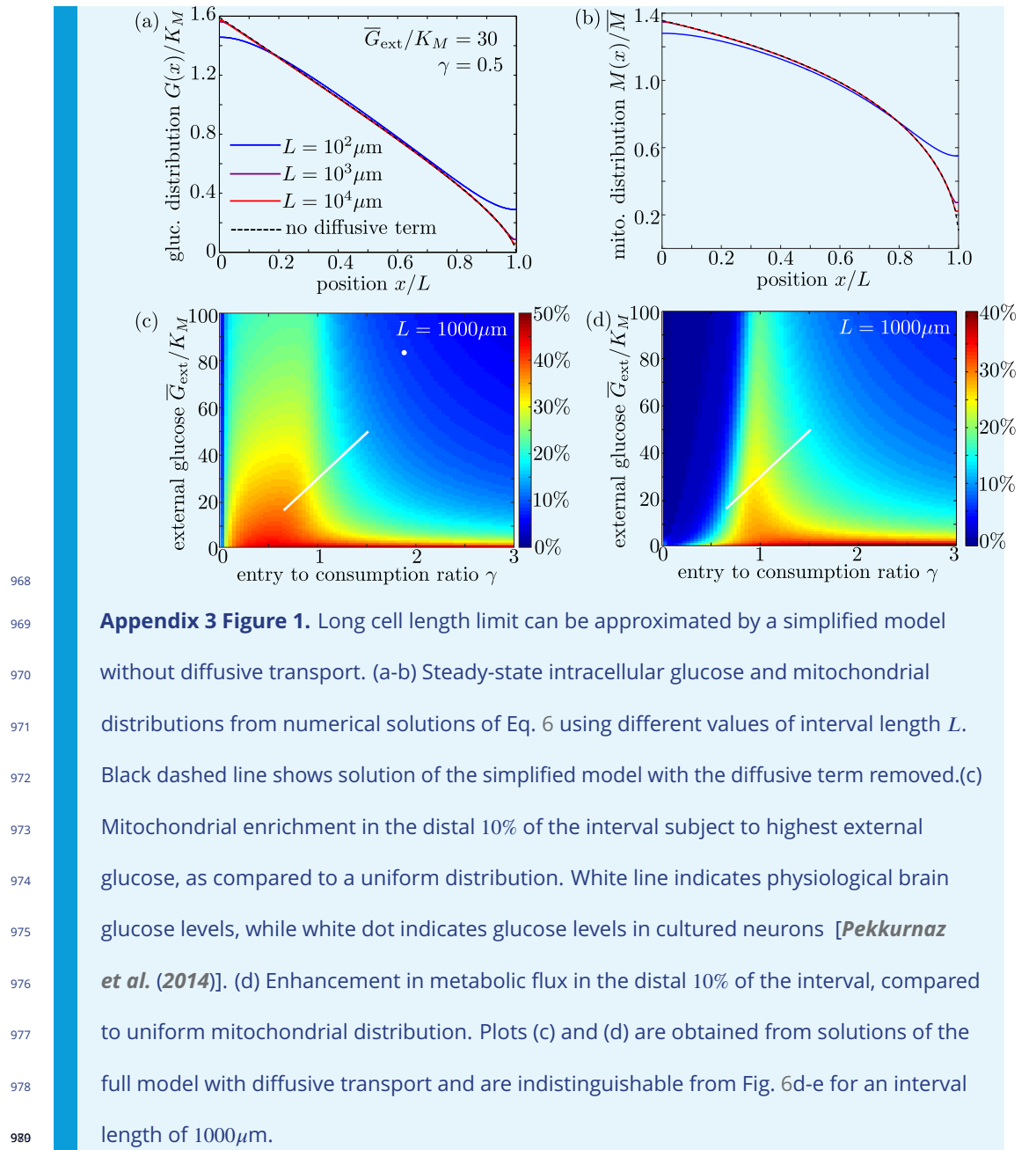
(a) *Duffieux et al. (2000)*; (b) *Kahana et al. (1960)*; (c) *Li et al. (2007)*; (d) *Urbina and Crespo (1984)*

Appendix 3

Effect of domain length L in uniform permeability model

Dimensional analysis of Eq. 6 indicates that the diffusive term for glucose dynamics will be negligible compared to the consumption and entry terms in the limit $L \gg \sqrt{D(G + K_M)/(k_g \bar{M})}$. We assume that external glucose concentrations are well below 10mM, indicating that the diffusive term is irrelevant for $L \gg 150\mu\text{m}$. If diffusion is neglected, the only length units in the model are found within external glucose and mitochondrial concentrations, both of which are fixed parameters independent of axonal length. We therefore expect in this limit that the model results will not depend on the interval length L .

To verify the accuracy of this limit, we plot glucose and mitochondrial distributions for the full model (including diffusion) for interval lengths of $L = 100\mu\text{m}$, 1mm 1 cm (Appendix 3, Fig. 1a,b). All other parameters are from our physiological estimates in Table(1). We note that for lengths well above $100\mu\text{m}$, the distributions are independent of L and are nearly identical to those expected for the model with diffusion excluded. We also plot mitochondrial accumulation and metabolic enhancement in the distal 10% of the interval obtained from solutions of the full model with diffusive transport, which match well to the plots in the main text (Fig.6) that neglect diffusive transport. We can thus assume that glucose entry and turnover are much faster than diffusive spread for biologically relevant parameter regimes.



Appendix 3 Figure 1. Long cell length limit can be approximated by a simplified model without diffusive transport. (a-b) Steady-state intracellular glucose and mitochondrial distributions from numerical solutions of Eq. 6 using different values of interval length L . Black dashed line shows solution of the simplified model with the diffusive term removed. (c) Mitochondrial enrichment in the distal 10% of the interval subject to highest external glucose, as compared to a uniform distribution. White line indicates physiological brain glucose levels, while white dot indicates glucose levels in cultured neurons [Pekkurnaz *et al.* (2014)]. (d) Enhancement in metabolic flux in the distal 10% of the interval, compared to uniform mitochondrial distribution. Plots (c) and (d) are obtained from solutions of the full model with diffusive transport and are indistinguishable from Fig. 6d-e for an interval length of $1000 \mu\text{m}$.

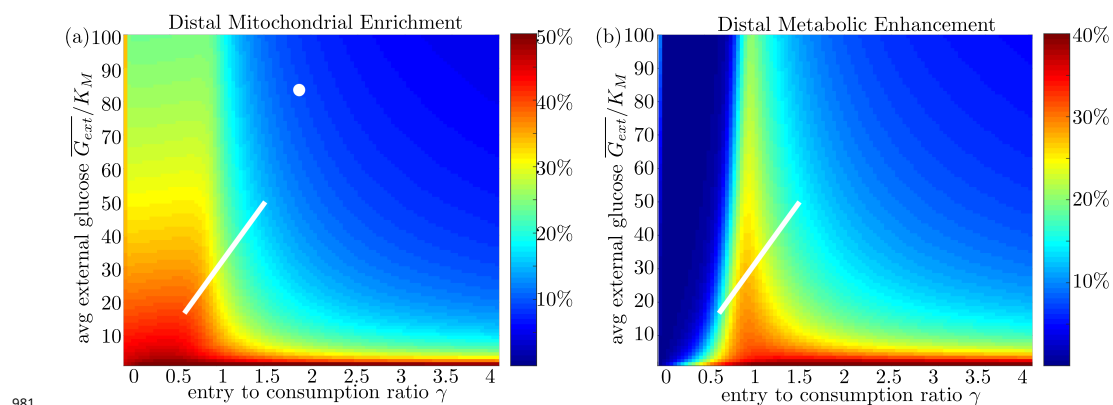


Figure 6–Figure supplement 1. High stopping rate limit for model with uniform glucose permeability. For the high k_s limit, we show (a) mitochondrial enrichment in the distal region and (b) metabolic enhancement in the distal region. In this limit, mitochondrial accumulation occurs for arbitrarily low values of γ as nearly all mitochondria are in the stopped state even at very low internal glucose concentrations. However, metabolic enhancement still occurs only within a narrow range of γ values.